~~Driving mechanisms of the dissolved~~Dissolved oxygen budget in the Levantine Sea: a coupled physical-biogeochemical modelling approach

Joelle Habib[1,2,3], Caroline Ulses[1], Claude Estournel[1], Milad Fakhri[3], Patrick Marsaleix[1], Thierry Moutin[4], Dominique Lefevre[4], Mireille Pujo-Pay[5], Marine Fourrier[2], Laurent Coppola[2,6] , Cathy Wimart-Rousseau[7] and Pascal Conan[5,6]~~†~~*

[1]Laboratoire d'Etudes en Géophysique et Océanographie Spatiales (LEGOS), Université de Toulouse, CNES/CNRS/IRD/UT3, 14 avenue Edouard Belin, 31400 Toulouse, France
[2]Sorbonne Université, CNRS, Laboratoire d'Océanographie de Villefranche, LOV, 06230 Villefranche-sur-Mer, France
[3]National Center for Marine Sciences, National Council for Scientific Research (CNRS-L), Jounieh, Lebanon
[4] Aix Marseille Univ, Université de Toulon, CNRS, IRD, MIO, Marseille, France
[5]Laboratoire d'Océanographie Microbienne (LOMIC), CNRS, UMR 7621, Sorbonne Université, 1 Avenue Pierre Fabre, 66651 Banyuls-sur-mer, France
[6]Sorbonne Université, CNRS OSU STAMAR – UAR2017, 4 Place Jussieu, 75252 Paris, France
[7]National Oceanography Centre Southampton, European Way, Southampton, SO14 3ZH, UK

~~†~~* Deceased

Correspondence to: Joelle Habib (joellehabib22@hotmail.com)

Abstract.

The Levantine Basin is an ultra-oligotrophic region and the formation site of ~~the~~ Levantine Intermediate ~~Waters. For the first time, a~~Water. A high-resolution 3D coupled hydrodynamic-biogeochemical model~~,~~ (SYMPHONIE-Eco3MS~~,~~) was used to investigate the seasonal and interannual variability of dissolved oxygen (O_2) in the Levantine Basin and to estimate its basin-wide budget ~~for~~over the period 2013–2020. ~~Our~~The model results show ~~that the simulated O_2 concentrations align well with *in situ* data from research cruises and Argo floats.~~a pronounced seasonal cycle of air-sea exchanges. During winter, cooling and vertical mixing induce an undersaturation in oxygen of the surface layer ~~is undersaturated in oxygen~~ by up to 2% across the entire basin, leading to atmospheric oxygen absorption. ~~The model~~ In contrast, during the stratified period, primary production and warming induce a slight oversaturation and subsequent oxygen release to the atmosphere. The annual budget over the 7-year period shows that ~~on an annual scale,~~ the basin acts as a net sink for atmospheric oxygen~~, with the Rhodes Gyre exhibiting uptake rates twice as high as the rest of the Levantine Basin. The~~ . The oxygen budget analyses further indicate that the surface layer ~~also serves~~(0-150m) acts as a source of dissolved oxygen for intermediate depths~~, with 4.2 ± 1.1 mol m^{-2} year^{-1} of dissolved oxygen vertically transported. Oxygen is transported laterally~~ through winter vertical export, whose amplitude is significantly governed by the magnitude of heat fluxes. At the basin and annual scale, we estimate a net lateral oxygen input into the basin from the Ionian Sea and ~~exported~~a net export towards the Aegean Sea, with ~~winter~~

Style Definition: Heading 1
Style Definition: Heading 2
Style Definition: Heading 3
Style Definition: Heading 4
Style Definition: Heading 5
Style Definition: Heading 6
Style Definition: Title
Style Definition: Subtitle
Formatted: Numbering: Continuous

~~heat loss intensity enhancing~~ this lateral export at both surface and intermediate layers~~. The~~ enhanced when winter heat loss is intense. Biogeochemically, the Levantine Basin alternates between autotrophic and heterotrophic states on an annual basis, depending on the intensity of winter surface heat loss. Spatially, the Rhodes Gyre, a quasi-permanent cyclonic structure and major site of intermediate water formation, emerges as a significant oxygen pump in winter, with annual uptake rates twice as high as the rest of the Levantine Basin, and shows enhanced biological production during the productive season, contributing to 41% of the ~~total~~net annual oxygen production in the surface layer in the ~~Levantine~~ basin. This study highlights the need for further modeling studies on pluri-annual and multi-decadal scales to explore ~~the~~ interannual variability and evolution of the annual oxygen budget across the entire Eastern Basin, particularly in the context of climate change.

1 Introduction

Formatted: Font colour: Auto

Dissolved oxygen (O_2) is essential for marine life, supporting respiration of living organisms and the oxidation of organic matter, thereby regulating nutrient cycling and ~~therefore~~organic matter remineralization, and influencing the biogeochemical cycles of important elements in the ocean~~.~~ (Breitburg et al., 2018; Gruber, 2011; Morée et al., 2023). The ocean's oxygen inventory is primarily controlled by its production through photosynthesis, ~~respiration of organic matter,~~and its consumption through remineralization, as well as by temperature and salinity-dependent oxygen solubility, air-sea exchange and the mixing and advective fluxes influencing the ventilation of water masses~~.~~ (Sanders et al. 2026; Helm et al, 2011). Since 1960, the total oxygen inventory has decreased by 2% in the Global Ocean (Schmidtko et al., 2017)~~. This decrease in oxygen inventory referred to as deoxygenation has been~~, a decline primarily attributed to ~~the global~~ warming~~ which leads to the reduction of~~-induced reductions in oxygen solubility~~, explaining ~15% of the current total global oxygen loss (Schmidtko et al., 2017),~~ and ~~the increase of~~to enhanced upper~~-~~-ocean stratification~~ generating a reduction of~~, which limits vertical ventilation~~ and circulation of deep ocean layers~~ (Helm et al., 2011; Schmidtko et al., 2017~~).~~; Breitburg et al., 2018; Stramma and Schmidtko, 2021). However, oxygen changes present large regional and temporal ~~variability~~ heterogeneity (Schmidtko et al., 2017; ~~Stramma and Schmidtko, 2021~~Levin, 2018, Feucher et al., 2022; Kolodziejczyk et al., 2024; Wu et al, 2025)~~. The decline in oxygen inventory induced by global warming, combined with seasonal, interannual, and decadal variations, is barely detectable~~, making long-term trends difficult to detect in the upper ~~layer~~ocean. Identifying the relative contribution of ~~the water column. The description and assessment of the various~~physical and biogeochemical drivers ~~and processes influencing oxygen changes may provide valuable insight into the complex~~is therefore essential to better understand regional ~~variations in~~ oxygen dynamics.

~~The objective of the present work is to assess the main mechanisms controlling the oxygen changes and budget in the ultra-oligotrophic south-eastern Mediterranean Sea at seasonal and interannual time scales over 7 years. The Mediterranean Sea is a well-ventilated basin compared to the World Ocean (Schneider et al., 2014; Tanhua et al., 2013). The low salinity Atlantic Water (AW) enters the surface layer through the Gibraltar Strait and travels towards the eastern sub-basin. It gradually transforms into a more saline Mediterranean Water due to the air-sea heat and moisture fluxes (Malanotte-Rizzoli et al., 2014). Reaching the Levantine Basin (Fig. 1), the Modified AW (MAW) subducts under the warm and saline Levantine Surface Water (LSW) in summer. During winter, surface heat loss increases water density, triggering vertical mixing that reaches intermediate depths and leads to the formation of the Levantine Intermediate Water (LIW). The Rhodes Gyre, a permanent cyclone in the northwest of the Levantine Basin (Lascaratos et al., 1999; Lascaratos and Nittis, 1998; Sur et al., 1993), has been identified as the main area of LIW~~

~~formation. Then, LIW propagates between 200-600 m in the whole Mediterranean (Brasseur et al., 1996). This water impacts the deep water formation in both the Adriatic Sea (Gačić et al., 2010; Lascaratos et al., 1999) and the Gulf of Lion (Schneider et al., 2014), acting as a preconditioning factor for these water formations with its high salinity. Part of LIW also exits the Mediterranean Sea, flowing toward the Atlantic.~~

~~The Levantine Basin is considered an ultra-oligotrophic region, except the Rhodes Gyre, where winter vertical convection enriches the surface layer with nutrients, stimulating organic carbon production (D'Ortenzio et al., 2021; Lavigne et al., 2013) and its export to the intermediate and surrounding areas (Habib et al., 2023). Previous studies have investigated the oxygen distribution and dynamics in this region (Di Biagio et al., 2022; Klein et al., 2003; Manca et al., 2004; Mavropoulou et al., 2020; Schlitzer et al., 1991; Tanhua et al., 2013). The vertical distribution in the basin is characterized by a surface layer exhibiting seasonal variability. During the stratified period, the upper waters present an oversaturated surface water and a sub-surface oxygen maximum (235 µmol kg^{-1}) between 50-80 m (Di Biagio et al., 2022; Kress et al., 2003; Mavropoulou et al., 2020), attributed to various processes such as primary production within that layer, or alternatively, downward transport mechanisms like subduction (Di Biagio et al., 2022). In winter, the oxygen vertical profile shows an upper mixed layer with maximum dissolved concentrations of 240 µmol kg^{-1}, characterised by an undersaturation in oxygen at the surface related to the atmosphere. At intermediate depths, the LIW oxygen has values ranging from 197 to 210 µmol kg^{-1} (Mavropoulou et al., 2020). An Oxygen Minimum Layer (OML) is located between 600-1200 m with a minimum concentration of 170/180 µmol kg^{-1} (Tanhua et al., 2013). Below this layer, deep waters originating from the Adriatic and Aegean seas present values above 185 µmol kg^{-1}, slightly higher than the ones recorded for the OML (Mavropoulou et al., 2020).~~

~~The Levantine Basin shows spatial changes in oxygen content occurring at short, annual, and decadal time scales (Kress et al., 2014; Sisma-Ventura et al., 2016). The modeling study by Cossarini et al. (2021) showed a negative trend in oxygen concentration at the surface of the Mediterranean Sea due to the surface temperature increase over the past two decades (Escudier et al., 2021; Ozer et al., 2016; 2022). Mavropoulou et al. (2020) highlighted a variability in deep and intermediate layers' oxygen concentration linked to shifts in the formation location of water masses between the Adriatic and the Aegean seas. In particular, in the 1990s, during the Eastern Mediterranean Transient (EMT), warmer, saltier, and more oxygenated waters originating from the Aegean Sea flowed into the deep layers of the Levantine Basin (Lascaratos et al., 1999). A net decrease in the oxygen inventory in deeper layers (1200-2000 m) of the southeastern Levantine Basin over the 20 years from 2002 to 2020 has also been pointed out by Sisma-Ventura et al. (2021), reflecting a return to pre-EMT state due to mixing between Aegean and Adriatic waters.~~ The Levantine Basin, in the south-easternmost Mediterranean Sea (Fig. 1) is an ultra-oligotrophic region characterized by exceptionally low primary productivity (Kress and Herut, 2001) and is particularly sensitive to changes in ventilation and biogeochemical processes. As the area of the formation of the Levantine Intermediate Water (LIW) which subsequently supplies the Eastern Intermediate Water (EIW), propagating throughout the entire Mediterranean Sea at intermediate depths (Brasseur et al., 1996), the Levantine Basin plays a crucial role in basin-scale ventilation (Kress et al., 2003). Its vertical structure of dissolved oxygen reflects the complex interplay of physical, biological, and chemical processes occurring at several temporal and spatial scales. The surface and intermediate waters characterized by exchanges with the atmosphere are well oxygenated, with a pronounced ventilation in the Rhodes Gyre, a permanent cyclone in the northwest of the basin, which has traditionally been identified as the major area of LIW formation (Lascaratos et al., 1999; Lascaratos and Nittis, 1998; Sur et al., 1993). The upper layer (0-150m) exhibits seasonal variability, with maximum oxygen values located in the mixed layer in winter, while during the stratification period, a subsurface oxygen maximum layer develops near 80 m depth, mostly attributed to both physical trapping of oxygen in Atlantic Water and biological production (Kress and Herut, 2001; Di Biagio et al., 2022). Beyond the seasonal signal associated with local processes, the properties of the upper layer are also influenced by the general eastern Mediterranean circulation and in particular the Adriatic-Ionian Bimodal Oscillation System (BiOS) (Gacic et al., 2010, 2011; Velaoras et al. 2014; Menna et al., 2022), characterized by two alternating circulation regimes: during the anti-cyclonic phase of the Northern Ionian Gyre (NIG), Atlantic Water (AW) flowing across the Sicily Channel is preferentially directed northwards, toward the Adriatic Sea, while during its cyclonic phase, AW, directed eastward, mostly supplies the Levantine Basin. The BiOS process presents quasi-decadal variability and has been proposed as a driver of changes in the thermohaline and biogeochemistry in the Adriatic and Levantine seas (Civitarese et al., 2010; Velaoras et al. 2014; Ozer et al., 2017; Ozer et al., 2022; Di Biagio et al., 2023; Civitarese et al., 2023). Below the euphotic layer, oxygen concentrations decline with an Oxygen Minimum Layer (OML) located below the Intermediate Water between 600 and 1200 m (Cardin et al., 2015; Mavropoulou et al., 2020) and characterized by concentrations of 170/180 µmol kg^{-1} (Tanhua et al., 2013). Deep water masses of the sub-basin are sensitive to variations in deep-water formation and circulation taking place in the Eastern Mediterranean. After the Eastern Mediterranean Transient (EMT) in the early 1990's when the deep water formation area shifted from the Adriatic to the Aegean Sea, an increase of oxygen was documented in the deeper layers in response to the inflow below 2500 m of more oxygenated waters originating from the Aegean Sea (Lascaratos et al., 1999; Mavropoulou et al., 2020). This was accompanied with the upward displacement of the older Adriatic-origin deep waters and of the OML. More recent observations, however, indicate a deoxygenation trend since 2008, attributed to weakened deep water formation and reduced ventilation rates as a progressive return to pre-EMT characteristics with an homogenized deep layer (Sisma-Ventura et al., 2021).

To date, ~~the oxygen inventory in the Eastern Mediterranean Basin remains poorly understood,~~ with limited spatial and temporal observations in the area, the variability of oxygen inventory in the Levantine Basin~~,~~ remains poorly understood, and there is no proposed comprehensive budget quantification for the entire region. ~~The~~In the framework of the PERLE (Pelagic Ecosystem Response to Deep Water Formation in the Levant Experiment~~) project aimed to gain insights into the biogeochemical cycles in this region through multi-platform observations and modelling. The objective of the present work is to assess the main mechanisms controlling the oxygen changes and budget in the ultra-oligotrophic south-eastern Mediterranean Sea at seasonal and interannual time scales over 7 years. In this study, we quantify~~, Conan and Durrieu De Madron, 2019) project, the present work aims at quantifying the seasonal and interannual variations in the oxygen inventory of the Levantine surface and intermediate water masses, detailing the contribution of air-sea oxygen fluxes, ~~biological~~biogeochemical and physical ~~processes~~fluxes. This analysis is based on 3D coupled hydrodynamic-biogeochemical model outputs covering a period of 7 years, from 2013 to 2020. Following on the budget approach developed by Ulses et al. (2021) for the north-western Mediterranean Sea, we investigate the ultra-oligotrophic Levantine Basin and provide a basin-scale quantification of its dissolved oxygen budget, highlighting the role of transport processes and permanent circulation features such as the Rhodes Gyre.

After the introduction (Sect. 1), this paper is organized as follows. Sect. 2 describes the coupled hydrodynamic-biogeochemical model implemented in the Levantine Basin and ~~observations used for the model assessment. Sect. 3 first presents~~ an assessment of the model results using *in situ* observations. Sect. ~~, then~~3 investigates the seasonal and interannual dynamics of oxygen in the surface and intermediate layers for the Levantine Basin, ~~describes its spatial~~

~~variability, and finally~~ estimates an annual budget of oxygen, and finally describes its spatial variability. This section is followed by a discussion of the results and a conclusion in Sect. 4 and 5, respectively.

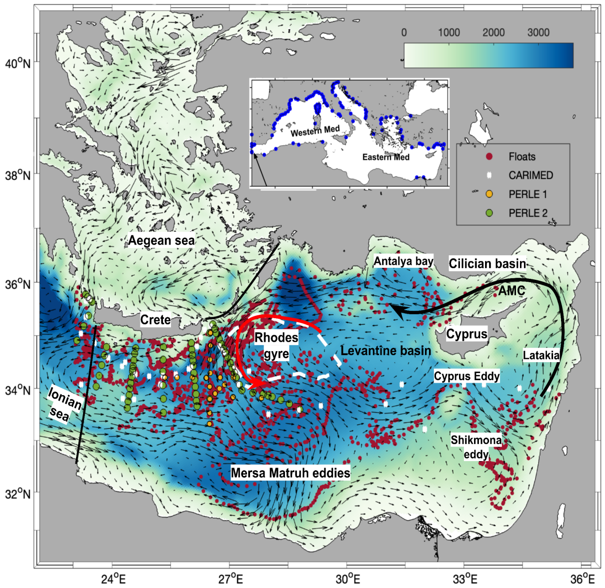

Figure 1: Model domain and bathymetry (m, background) in the Eastern Mediterranean. The arrows represent the simulated surface currents averaged over the study 7-year period (2013-2020), black thick lines delimit the basin for the budget calculation. Red, yellow, and green dots indicate BGC-Argo floats trajectories, PERLE-1, and PERLE-2 cruise stations, respectively, and white crosses CARIMED cruise stations, over the period from 2013 to 2021. Blue dots in the insert represent the river mouths.

2. Material and Method

2.1 Modeling

2.1.1 The coupled hydrodynamic-biogeochemical model

~~The modeling presented in this study is based on the biogeochemical model Eco3M-S forced offline by the ocean circulation model SYMPHONIE, described in detail in Marsaleix et al. (2006, 2008), Estournel et al. (2016), and Damien et al. (2017). This latter is a 3D primitive equation model with a free surface and generalized sigma vertical coordinate previously used to simulate the hydrodynamic conditions of the Mediterranean Sea: in river plumes~~

~~(Estournel et al., 1997, 2001; Marsaleix et al., 1998), for dense water formation (Estournel et al., 2005, 2016; Herrmann et al., 2008; Ulses et al., 2008) and shelf-slope exchanges (Mikolajczak et al., 2020).~~

~~We used the biogeochemical model~~ This study is based on a Mediterranean configuration of the ocean circulation model SYMPHONIE (Marsaleix et al. 2006; 2008), forcing offline the biogeochemical model Eco3M-S (Ulses et al., 2016; 2023). The horizontal resolution of the model grid varies from 2.3 to 4.5 km, with a refined resolution of 1.3 km in the Gibraltar Strait. The vertical grid has 60 vertical vanishing quasi sigma levels. More details can be found in Estournel et al. (2021).

Eco3M-S~~,~~ is a multi-nutrient and multi-plankton functional type model, representing the dynamics of the pelagic plankton ecosystem and the cycles of carbon, nitrogen, phosphorus, silicon, and oxygen ~~(Auger et al., 2011; Ulses et al., 2023). The phytoplankton is represented by three size classes: pico-, nano-, and micro-phytoplankton (named class 1, 2, and 3, respectively), with variable internal ratios. The zooplankton is also represented by three size classes: nano-, micro-, and mesozooplankton (named class 1, 2, and 3, respectively). A compartment of bacteria has been explicitly taken into account. The internal composition varies for phytoplankton and remains constant for heterotrophic organisms. Four dissolved inorganic nutrients have been considered: nitrate, ammonium, phosphate, and silicate. In addition to dissolved organic matter (DOM), particulate organic matter (POM) has been divided into two weight classes, namely light and heavy. The biogeochemical model was previously used to study the dynamics of the planktonic ecosystems and organic carbon (Auger et al., 2014; Herrmann et al., 2013; Kessouri et al., 2018; Many et al., 2021; Ulses et al., 2016), as well as the nitrogen and phosphorus cycles (Kessouri et al., 2017), and the oxygen dynamics (Ulses et al., 2021) in the northwestern Mediterranean Sea.~~(Auger et al., 2011; Ulses et al., 2023), with 37 state variables. The rate of change of dissolved oxygen concentration due to biogeochemistry in the water column is calculated based on the following equation:

$$\frac{dDOx}{dt} = \sum_{i=1}^{3} (GPP_i - RespPhy_i)\gamma_{C/DOx} - \sum_{i=1}^{3} (RespZoo_i)\gamma_{C/DOx} - RespBac\,\gamma_{C/DOx}$$

$$+ (UptPhy_{i,NO_3} - Nitrif)\gamma_{NH_4/DOx} \qquad \text{(Eq. 1)}$$

The dissolved oxygen concentration is represented by the term DOx. GPP_i and $RespPhy_i$ are gross primary production and respiration, respectively, for phytoplankton group i. $RespZoo_i$ and RespBac are respiration of zooplankton group i and of bacteria, $UptPhy_{i,NO3,}$ and Nitrif uptake of nitrate by phytoplankton class i, and nitrification, respectively. $\gamma_{C/DOx}$ and $\gamma_{NH_4/DOx}$, equal to 1 and 2, respectively, are the moles of DOx used per mole of C in respiration and needed to oxidize one mole of ammonium in nitrification as described in Grégoire et al. (2008). The flux of dissolved oxygen at the air-sea interface is calculated using the Garcia and Gordon (1992) equation for the solubility, and the parametrization of Wanninkhof and McGillis (1999) for the transfer velocity, following the study of Ulses et al. (2021) in the northwestern Mediterranean deep convection area.

~~The flux of dissolved oxygen at the air-sea interface is governed by the following equation:~~

~~$DOxFlux = Kw(DOxSat - DOxSurf)$ (Eq. 2)~~

~~$DOxSat$ represents the oxygen saturation also known as solubility and $DOxSurf$ the concentration of dissolved oxygen at the surface. The dissolved oxygen at solubility level is determined using the Garcia and Gordon (1992) equation. The oxygen saturation anomaly (OSA, expressed in percentage) is defined as the difference between the dissolved oxygen concentration and the solubility: $(DOx - DOxSat)/DOxSat$ x100 %. Kw represents the O_2 transfer velocity in m s^{-1}. We used the parametrization of Wanninkhof and McGillis (1999) with a cubic dependency to the 10-m wind speed following the study of Ulses et al. (2021) in the northwestern Mediterranean deep convection area, which obtained the best fits with in situ observations of oxygen concentration using this parametrization.~~

~~2.1.2 Implementation~~

2.1.2 Initialisation and boundary conditions

The implementation of the coupled ~~physical-biogeochemical~~ model was described in detail in Estournel et al. (2021) and Habib et al. (2023)~~. The hydrodynamic model covers the Mediterranean Sea and the Marmara Sea and it extends to 8° west in the Gulf of Cadiz.The horizontal resolution varies between 2.3 and 4.5 km, in general. A narrowing was conducted in the Gibraltar Strait with a 1.3 km grid for a better representation of the exchange area between the Mediterranean Sea and the Atlantic Ocean. The model has 60 vertical vanishing quasi sigma levels (Estournel et al., 2021) with closer levels near the surface.~~. The period simulated by the hydrodynamic model runs from May 2011 to May 2021. ~~This model configuration was used to describe the surface and intermediate water circulations in the eastern Mediterranean Sea (Estournel et al., 2021).~~ Atmospheric forcings for both hydrodynamic and biogeochemical models were provided by the HRES (atmospheric model High RESolution forecast) product of ECMWF model with a horizontal resolution of 1/8° using hourly fields (wind, air temperature and humidity, pressure, solar and downward longwave radiation, and precipitation). ~~The model accounts for a total of 142 rivers (Fig. 1).~~

The biogeochemical model Eco3M-S was forced by daily fields of temperature, salinity, current, and vertical diffusivity from the SYMPHONIE model. It covers the period between August 2011 till March 2021. The ~~two~~ first two years ~~for~~(July 2011–December 2013) of the biogeochemical simulation were dedicated to model ~~were considered as a~~ spin-up to ensure biogeochemical stability and were not considered in the analysis~~. We used wind speed~~, while the December 2013– December 2020 period was used for the budget analysis. This period was selected based on the availability of consistent physical forcing and ~~solar radiation atmospheric forcings provided by the ECMWF~~ the density of in situ observations for model ~~as for the hydrodynamic simulation~~initialization and validation. The biogeochemical model was initialized using climatological fields of in situ nutrient and dissolved oxygen concentrations from the CARIMED (CARbon in the MEDiterranean Sea, Alvarez et al., 2019) database and Biogeochemical-Argo (BGC-Argo) float data over the 2011-2012 summer periods when data were available, in 10 sub-regions. At the ~~river~~ mouths~~,~~ of 142 rivers taking into account (Fig. 1), concentrations of nutrients were imposed by sub-basin using the dataset of Ludwig et al. (2010). Dissolved oxygen at river mouths was set at saturation values. In the Atlantic Ocean, nutrients were prescribed using monthly profiles from the World Ocean Atlas 2009 climatology at 5.5 °W. In the Marmara Sea, to represent a two-layer flow regime, we imposed a daily relaxation towards a nutrient concentration of 0.24 and 1.03 mmol N m^{-3} and a phosphate concentration of 0.06 and 0.05 mmol P m^{-3} for depths above and below 15 m, respectively, based on the observations near the Dardanelles Strait from (Tugrul et al., 2002).

Formatted: Font: Not Italic

2.1.3 ~~Study area and budget~~Budget calculation

~~The study~~For spatial mean and budget calculation, we defined an area (delimited by the black lines~~,~~ in Fig. 1) ~~covers~~covering 540 000 m^2~~. For spatial mean and budget calculation, the~~, with the boundary with the Ionian Sea linking the southwestern Cretan coast to the Libyan coast. The water column was divided into three layers based on the thermohaline structure represented by the physical model (Estournel et al., 2021) and the associated dominant biogeochemical processes ~~as well the depth of the LIW~~: the surface layer defined as the photic layer covering the surface to 150 m depth where photosynthesis takes place, the underlying intermediate layer from 150 to 400 m where LIW flows, and the deep layer below 400 m ~~(Estournel et al., 2021).~~. In this study, we will be focusing on the first two layers~~, as~~ where changes ~~at greater depths are very slow over the 8-year period and barely detectable~~, in particular related to LIW formation, occur generally more rapidly. The biogeochemical term of the oxygen budget is the sum of oxygen production due to gross primary production and nitrate uptake by phytoplankton, and of oxygen consumption through nitrification and community respiration. The physical term is divided into two components: the lateral and the vertical transports, which are both due to advection and mixing processes. The lateral transport represents the exchanges at the boundaries with the Ionian and Aegean seas. A negative lateral transport indicates a net export of oxygen from the considered layer of the Levantine Basin. The oxygen inventory, air-sea fluxes, biogeochemical fluxes, and lateral fluxes were calculated online while the vertical transport, defined as a net flux at the layer interface, was deduced from the other terms of the budget. The budget calculation is detailed in Text S1 in Supplement Material.

Formatted: Font colour: Auto

Formatted: Font colour: Auto

Formatted: Font colour: Auto

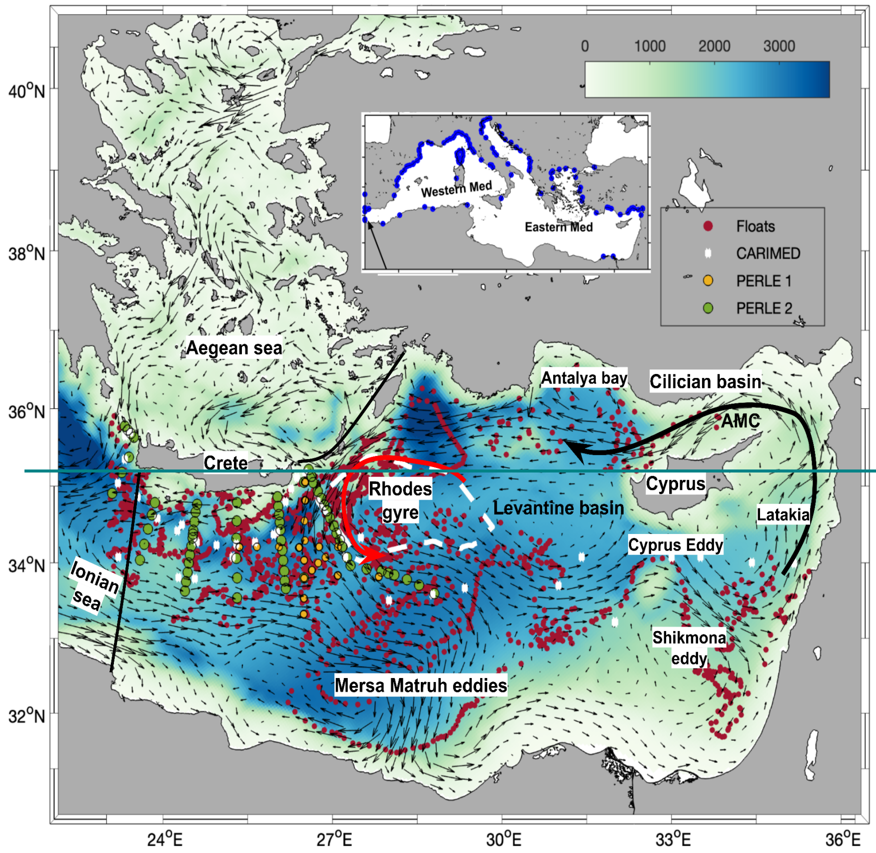

~~**Figure 1: Model domain and bathymetry (m, background) in the Eastern Mediterranean. The arrows represent the simulated surface currents averaged over the study 7-year period (2013-2020), black thick lines delimit the basin for the budget calculation. Red, yellow, and green dots indicate BGC-Argo floats trajectories, PERLE-1, and PERLE-2 cruise stations, respectively, and white crosses CARIMED cruise stations, over the period from 2013 to 2021. Blue dots in the insert represent the river mouths.**~~

2.2~~.2 Observations for model~~ Model assessment

~~2.2.1. Argo float data~~

~~In order to assess the modeled temporal and spatial evolutions of the oxygen concentration, we use observations from Argo floats that were deployed in the Levantine Basin during the periods of 2013-2015 and 2015-2018. In particular,~~

~~we present comparisons with data provided by the two BGC-Argo floats 6901528 and 6901764 (151 and 173 vertical profiles, respectively). Temperature and salinity measurements were also extracted to calculate oxygen solubility. The oxygen data were downloaded from the Argo Global Data Assembly Center web portal accessible through the Coriolis database (http://www.coriolis.eu.org). Calibration of dissolved oxygen was performed at the deployment using in situ observations from 0 to 1000 m depth (Winkler titration). The calibration and the deployment strategy are detailed in (Thierry et al., 2021). The uncertainties of the measurements were estimated at ~ 2-10 µmol kg^{-1} depending on the sensor (Grégoire et al., 2021).~~

~~2.1.2 Cruise data and seawater measurements~~

~~During the period from October 2018 to March 2019, biogeochemical measurements were made in the context of PERLE (D'Ortenzio et al., 2021) in the Levantine Basin to describe the preconditioning and dispersion of the Levantine Intermediate Water (LIW) and to assess its role in structuring the phytoplankton ecosystem. In this study, we use data from two PERLE cruises: PERLE-1 (https://campagnes.flotteoceanographique.fr/campagnes/18000848/fr/) on board R/V l'Atalante in October 2018 and PERLE-2 on board R/V Pourquoi Pas? in February-March 2019 (Conan and Durrieu De Madron, 2019). PERLE-1 covers the period of the preconditioning of LIW formation during which an array of 25 CTD casts was set up. PERLE-2 covers the water formation period with 29 CTD-oxygen casts (Fourrier, 2020). Stations of PERLE cruises are indicated in Fig. 1. Winkler analyses were performed onboard using photometric endpoint detection to adjust the SBE43 raw data. After sensor coefficient adjustment, the accuracy of the SBE43 sensor is estimated to be around 2 µmol kg^{-1}.~~

~~We also use the observations included in the CARIMED database, collected during four cruises that covered the farthest east and south of the basin: the Meteor M84/3 (Tanhua, 2013), HOTMIX (Arístegui, J., & UTM-CSIC. (2018). HOTMIX Cruise, RV Sarmiento de Gamboa [Data set]. UTM-CSIC. http://doi.org/10.20351/29SG20140427 SMASH), MEDSEA (Ziveri and Grelaud, 2015), and MSM72 (Hainbucher et al., 2020) cruises conducted during the period between 2011-2018. The seawater was collected using Niskin bottles from the surface to 4600 m of depth using an SBE43 oxygen sensor for the oxygen concentrations, followed by the modified Winkler potentiometric method (Martínez-Pérez et al., 2017). The spatial coverage of the datasets is shown in Fig. 1.~~

~~3 Results~~

~~3.1 Assessment of the model~~

An assessment of the hydrodynamic ~~simulation was performed by Estournel et al. (2021), who showed the capacity of the model to reproduce the observed hydrology, as well as~~ and biogeochemical simulations in the surface and intermediate ~~circulations. In Habib et al. (2023), the results of the biogeochemical model were evaluated in terms of spatial and temporal variabilities of~~ water masses has been performed in previous studies (Estournel et al., 2021; Habib et al., 2023), suggesting its capacity to reproduce the observed general hydrology and biogeochemistry (chlorophyll, dissolved inorganic nutrients, and dissolved oxygen ~~against satellite, cruise, and BGC-Argo float data.~~) in the Levantine Sea. Here, ~~we~~the model is further ~~assess~~ assessed in terms of the dissolved oxygen dynamics by providing supplementary comparisons with ~~cruises, notably PERLE cruises, and Argo float data, as well as in~~ observations from BGC-Argo floats (6901528 and 6901764, http://www.coriolis.eu.org, Last access: 11 February

2026), PERLE cruises (PERLE-1 and PERLE-2, https://campagnes.flotteoceanographique.fr/campagnes/18000848/fr/, Last access: 5 June 2025, Conan and Durrieu De Madron, 2019), and those gathered in the CARIMED database (Alvarez et al., 2025), as well as from situ measurements of metabolic rates.

~~3.1.1 Comparison with BGC-Argo float data~~

~~Figure 2 represents the temporal evolution of vertical profiles of oxygen from both the model and float observations over the first 500 m, as well as the surface oxygen concentration and oxygen solubility along the float's pathways that were selected for their broad spatio-temporal coverage, each capturing stratification and mixing periods at different locations (Fig. 2a). The observations and the model outputs exhibit the same seasonal variability (Fig. 2 d,e). During summer, both oxygen solubility and surface oxygen concentrations reach their minimum values. Oxygen solubility starts increasing following this period (Fig. 2d-e). Modeled and observed surface oxygen concentrations and solubility show correlation coefficients higher than 0.95 (p-value < 0.05) with a bias lower than 3 µmol O_2 kg^{-1}. The RMSD values (Root Mean Square Difference) are less than 5 µmol O_2 kg^{-1} for both floats and fall within the oxygen uncertainty interval associated with Argo float data.~~

~~The general observed features across the water column are respected by the model (Fig. 2b-c) with (i) a subsurface oxygen maximum formation in March/April when the water column restratifies, (ii) a deepening of oxygen maximum until December, followed by (iii) the erosion of the oxygen maximum and homogenization of the surface layer when vertical mixing intensifies, inducing a relatively deep mixed layer. The oxygen maximum in the subsurface layer is underestimated by ~5 µmol kg^{-1} by the model ($\mathrm{RMSD} \simeq 8$ µmol kg^{-1}) for the period while its depth is well located. Further deep, the concentration and the localization of the OML are well reproduced with a magnitude of 180 µmol kg^{-1} and depths between 380 and 500 m (Fig. 2b-c). Overall, the simulation reproduces correctly the spatial and temporal variability of the oxygen observed at the surface and in the water column.~~

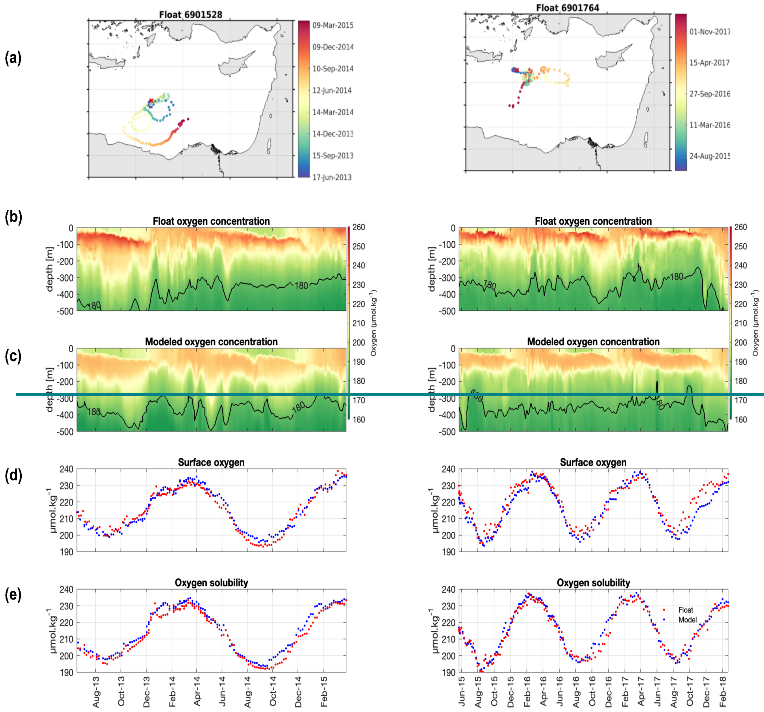(a)
Float 6901528
09-Mar-2015
09-Dec-2014
10-Sep-2014
12-Jun-2014
14-Mar-2014
14-Dec-2013
15-Sep-2013
17-Jun-2013
Float 6901764
01-Nov-2017
15-Apr-2017
27-Sep-2016
11-Mar-2016
24-Aug-2015
(b)
Float oxygen concentration
depth [m]
180
Oxygen (µmol.kg-1)
(c)
Modeled oxygen concentration
(d)
Surface oxygen
µmol.kg-1
(e)
Oxygen solubility
Float
Model
Aug-13
Oct-13
Dec-13
Feb-14
Apr-14
Jun-14
Aug-14
Oct-14
Dec-14
Feb-15
Jun-15
Aug-15
Oct-15
Dec-15
Feb-16
Apr-16
Jun-16
Aug-16
Oct-16
Dec-16
Feb-17
Apr-17
Jun-17
Aug-17
Oct-17
Dec-17
Feb-18

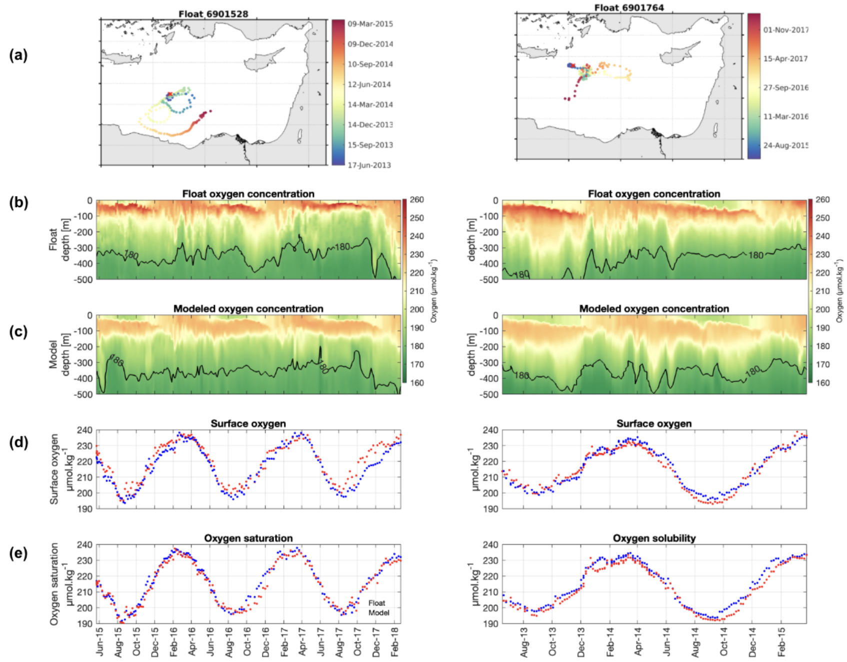

Figure 2: From top to bottom: (a) trajectory of the BGC-Argo floats with deployment position (red cross) and chronology in color; Hovmöller diagrams of oxygen concentration (µmol O_2 kg^{-1}) from (b) float data and (c) model outputs for the first 500 m; (d) surface oxygen concentration in the first 10 m (µmol O_2 kg^{-1}) and (e) oxygen solubility (µmol O_2 kg^{-1}), from the float data (red) and the model (blue).

Formatted: Font: Bold

The model reproduces the observed seasonal and vertical variability (Fig. 2, Fig. S1), with strong agreement with observations throughout the upper 500 m, in particular in the timing and depth of the subsurface oxygen maximum and the oxygen minimum layer. The discrepancies found concern a slight underestimation of the subsurface oxygen maximum (RMSD $\simeq$ 8 µmol kg^{-1}) compared to the BGC-Argo float, and an overestimation below 100 m compared to PERLE-2 observations, likely due to an overestimation of remineralization processes or vertical diffusion. The model and in situ data significantly correlate with correlation coefficient higher than 0.95 (p-value< 0.05). The RMSD values (Root Mean Square Difference) between modeled and observed surface oxygen and solubility are less than 5 µmol O_2 kg^{-1} for both Argo floats and fall within the oxygen uncertainty interval associated with Argo float data (~ 2-10 µmol kg^{-1} depending on the sensor, Grégoire et al., 2021). Finally, comparisons between model results with metabolic rate measurements near the surface and within the upper layer over the May-July period (BOUM cruise (Christaki et al. 2011); THRESHOLD cruises (Regaudie-de-Gioux et al., 2009); MINOS cruise (Moutin and Raimbault, 1996) indicate that modeled GPP (gross primary production), CR (community respiration) and NCP (net community production, corresponding to GPP minus CR) fall in the observed range, generally in their upper values (Table S1). These comparisons show the model's ability to represent oxygen-related biogeochemical processes in the Levantine Basin.

3 Results

~~3.1.2 Comparison with cruise data~~

~~Comparisons with data from PERLE-1, PERLE-2, and CARIMED cruises (Fig. S1) show that the model accurately reproduces the magnitude and variability of oxygen concentrations across the different water layers, consistent with observations from the floats comparison. The model and the data from PERLE1, PERLE2, and CARIMED significantly correlate (correlation coefficient higher than 0.95, p-value< 0.05). The model reproduces the intensity of the subsurface maximum reaching 230 µmol O_2 kg^{-1} during the PERLE-1 cruise in fall (Fig. S1a) contrary to its underestimation noted when comparing the model with the floats (Sect. 3.1.1). These differences between the floats and the cruise data and between the cruises (Fig. S2) could reflect differences in the sampling methods between each campaign of the dataset or mesoscale variability not correctly reproduced by the model.~~

~~The highest concentrations (230 µmol O_2 kg^{-1}) are located at the surface during the winter PERLE-2 cruise and CARIMED observations collected during the mixing period, for both model and observations (Fig. S1 b and d). Modeled dissolved oxygen concentrations below 100 m generally stand within the upper range of the observed values, except for the comparison with PERLE-2 observations, for which the model shows higher values all over the water column. The overestimation could be attributed to an overestimation of remineralization in this layer or vertical diffusion.~~

~~3.1.3 Comparison of process rates~~

~~Data on metabolic rates in the eastern Mediterranean Sea are scarce, and most available estimates are derived from observations made during stratified periods. Comparisons between model results averaged over periods from mid-June to mid-July and process rates measured near the surface and within the 145 m integrated layer in the core of an anticyclonic eddy in the eastern Levantine Basin during the BOUM cruise (Christaki et al., 2011) show that the modeled GPP, CR and NCP are in the upper range of the observational measurements. We also compared our model averages for May over the Levantine Basin with rates measured during the THRESHOLD cruises (Regaudie-de-Gioux et al., 2009) in the 5-110 m surface layer, and found values in the range of observations. In addition, model values integrated over the upper 100 m are consistent with those reported during the MINOS cruise (Moutin and Raimbault, 1996) conducted in the Levantine Basin between May and June. These comparisons can be found in Table 1.~~

~~**Table 1: Comparison between averaged modeled and observation rates over the same period and along the same region. a: Lagaria et al., (2011), b: Christaki et al. (2011), c: Regaudie-de-Gioux et al. (2009), (d) Moutin and Raimbault (1996).**~~

~~**Process**~~	~~**Campaign**~~	~~**Region**~~	~~**Period**~~	~~**Layer**~~	~~**Observation**~~	~~**Model**~~	~~**Reference**~~
~~**GPP**~~	~~BOUM~~	~~Core of an anticyclonic eddy in the~~	~~mid-June to mid-July~~	~~Near the surface~~	~~0.12 ± 0.90 mmol O_2 m^{-3} day^{-1}~~	~~1.36 mmol O_2 m^{-3} day^{-1}~~	~~a~~

		~~eastern Levantine~~		~~Integrated 145 m~~	~~28-75 mmol O_2 m^{-2} day^{-1}~~	~~68 mmol O_2 m^{-2} day^{-1}~~	~~b~~
	~~THRESHOLD~~	~~Levantine Basin~~	~~May~~	~~5-110 m~~	~~0.16-2.93 mmol O_2 m^{-3} day^{-1}~~	~~1-8 mmol O_2 m^{-3} day^{-1}~~	~~c~~
	~~MINOS~~	~~Levantine Basin~~	~~May to June~~	~~Near the surface~~	~~0.59 ± 0.16 mmol O_2 m^{-3} day^{-1}~~	~~1.08 mmol O_2 m^{-3} day^{-1}~~	~~d~~
			~~May to June~~	~~Integrated 100m~~	~~37.9 ± 4.8 mmol O_2 m^{-2} day^{-1}~~	~~37 mmol O_2 m^{-2} day^{-1}~~	~~d~~
~~**CR**~~	~~BOUM~~	~~Core of an anticyclonic eddy in the eastern Levantine~~	~~mid-June to mid-July~~	~~Near the surface~~	~~0.38 ± 0.92 mmol O_2 m^{-3} day^{-1}~~	~~1.28 mmol O_2 m^{-3} day^{-1}~~	~~a~~
				~~Integrated 145 m~~	~~39-58 mmol O_2 m^{-2} day^{-1}~~	~~68 mmol O_2 m^{-2} day^{-1}~~	~~b~~
	~~THRESHOLD~~	~~Levantine Basin~~	~~May~~	~~5-110 m~~	~~0.1-8.2 mmol O_2 m^{-3} day^{-1}~~	~~1-7 mmol O_2 m^{-3} day^{-1}~~	~~c~~
~~**NCP**~~	~~BOUM~~	~~Core of an anticyclonic eddy in the eastern Levantine~~	~~mid-June to mid-July~~	~~Near the surface~~	~~-0.26 ± 0.22 mmol O_2 m^{-3} day^{-1}~~	~~0.09 mmol O_2 m^{-3} day^{-1}~~	~~a~~
				~~Integrated 145 m~~	~~-4 ± 15 mmol O_2 m^{-2} day^{-1}~~	~~0.9 mmol O_2 m^{-2} day^{-1}~~	~~b~~
	~~THRESHOLD~~	~~Levantine Basin~~	~~May~~	~~5-110 m~~	~~-6.4-8.2 mmol O_2 m^{-3} day^{-1}~~	~~0-2 mmol O_2 m^{-3} day^{-1}~~	~~c~~

~~3.2~~3.1 Seasonal variability

~~3.2.1 Atmospheric forcing and vertical mixing~~

Figure 3 presents the mean annual cycle of the modeled air-sea heat flux, wind stress, mixed layer (ML) depth, and surface temperature, spatially averaged over the Levantine Sea from December 2013 to December 2020. During fall, the decrease in air temperature leads to significant sea surface heat loss, while intensified northern winds weaken stratification, gradually deepening the mixed layer (Fig. 3a-c). The sea surface temperature drops significantly (Fig. 3d). Heat loss events persist through winter, leading the surface temperature to reach a minimum of approximately 17°C and the mixed layer depth to gradually increase, peaking in January/February. The yearly maximum ML depth averaged spatially over the seven years is 108 ± 11 m (Table ~~S1~~S2). In March/April, the sea surface starts gaining heat, and the surface temperature increases (Fig. 3a and 3d). The ML abruptly shallows but still exhibits large variations during early spring, in response to the events of continental cold winds. The frequency of intense wind events decreases in late spring/summer (Fig. 3b). Surface temperature reaches maximum values around 28 °C in

August (Fig. 3d), and a thin ML settles until October. In the following, the annual cycle is divided into two successive periods based on the vertical mixing intensity. The first period is a mixing period, from October to March, and the second period is a stratified period, from April to September. The two periods were defined based on a mixed layer depth threshold of 25 m, following the criteria used by D'Ortenzio et al. (2008) and Houpert et al. (2015).

Formatted: Font colour: Auto

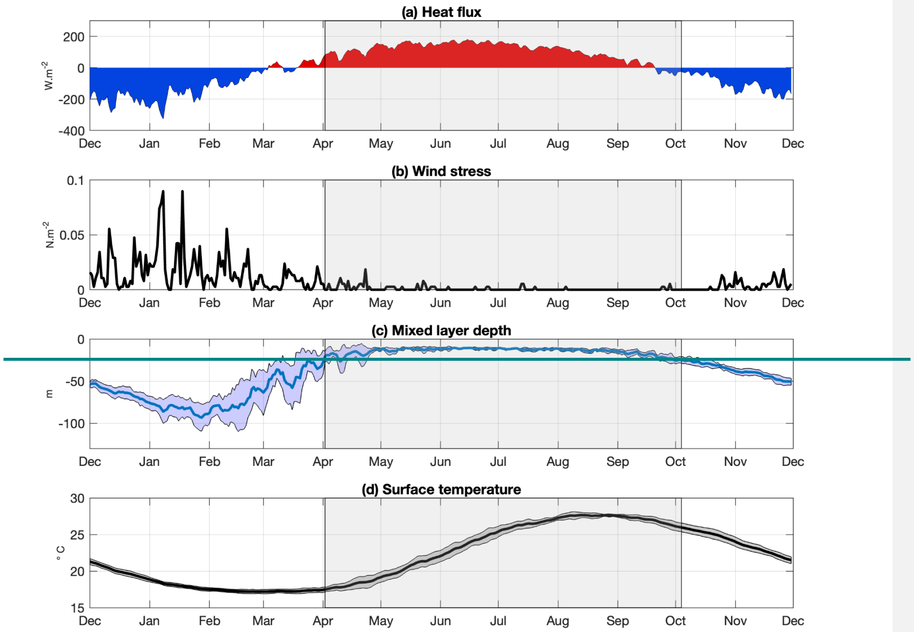

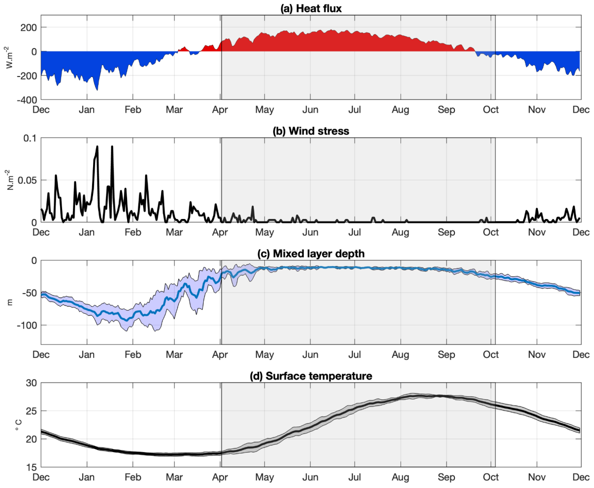

Figure 3: Annual time series of modeled (a) air-sea heat fluxes (W m^{-2}), (b) wind stress (N m^{-2}), (c) mixed layer depth (m), and (d) surface temperature (°C), averaged over the Levantine Sea and the period 2013-2020. In (c) **and (d), the solid line corresponds to the ~~spatial~~temporal mean, the shaded area to the standard deviation. The grey shaded area represents the stratification period.**

~~3.2.2 Oxygen fluxes~~

The annual cycle of the 7-year averaged oxygen fluxes and inventory ~~variation are described~~variations is shown in Fig. 4 and 5~~,~~ for the surface and intermediate layers, respectively. ~~The~~ In both layers, the oxygen content ~~in both layers~~ increases during the mixing period and gradually decreases during the stratified period, with minimum values in November/December for the surface layer and January for the intermediate layer (Fig. 4a and 5a). ~~The~~Both vertical and net horizontal transports ~~show~~exhibit a clear seasonal variation, ~~with the highest~~reaching maximum values of 50 mmol m^{-2} day^{-1} in ~~winter in~~ the surface layer and 50 mmol m^{-2} day^{-1} and 40 mmol m^{-2} day^{-1}, respectively in the intermediate layer (Fig. 4f and 5e). During the mixing period, ~~mostly~~and particularly during ~~intense wind~~events of strong winds and vertical mixing ~~events~~ (Fig. 3b-c), oxygen is exported from the surface layer towards the intermediate layer (Fig. 4f), and ~~then further down~~subsequently, from the intermediate towards the deep layer (Fig. ~~5e), with average~~5e). The associated mean export rates ~~of~~amount to 0.56 and 0.46 mol O$_2$ m^{-2} month^{-1}, respectively (Fig. S3b,d). During the stratified period, the downward export of O$_2$ towards the intermediate and deeper layers ~~decreases~~is reduced by 75% and 40%, respectively (Fig. S3d). ~~The~~

Horizontal oxygen ~~horizontal~~ transport in the surface layer is characterized by a net inflow from the Ionian Sea and an outflow towards the Aegean Sea (Fig. 4g, S2b~~), with higher values~~). These exchanges are stronger during the mixing period ~~compared to~~than during the stratified period (~~Ionian Sea:~~with inflow of 1.3 ~~vs~~versus 0.6 mol O$_2$ m^{-2} month^{-1}~~,~~ from the Ionian Sea and ~~Aegean Sea:~~outflow of 0.9 ~~vs~~versus 0.5 mol O$_2$ m^{-2} month^{-1} from the Aegean Sea, respectively, Fig. S3b). ~~The horizontal exchanges in~~In the intermediate layer ~~show~~, horizontal exchanges are weaker

Formatted: Subscript

overall but still display a ~~less intense pattern with~~seasonal signal. During the mixing period, a stronger net inflow from the Ionian Sea (0.2 mol O_2 m^{-2} $month^{-1}$) and a stronger outflow towards the Aegean Sea (-0.4 O_2 mol m^{-2} $month^{-1}$, Fig. S3d and 5f) ~~during~~are obtained. While the ~~mixing period. The~~ net oxygen ~~flow~~transport in the surface layer remains directed from the Ionian and towards the Aegean across both periods, ~~while~~ the intermediate layer exhibits net oxygen ~~outflow~~export toward both the Aegean and Ionian Seas ~~(~~during the stratified period, accounting for 96% and 4% of the total horizontal export~~) during the stratified period,~~ respectively (Fig. S3d).

~~The model~~Model results ~~show~~indicate that the ~~Levantine Basin~~ ecosystem in the surface layer ~~produces~~of Levantine Basin acts as a net source of dissolved oxygen from January to August, ~~at higher rates~~with the highest production between February and March~~, and consumes dissolved oxygen between~~. In contrast, net consumption dominates from September to December (Fig. 4d). ~~Biogeochemical~~Overall, the biogeochemical O_2 flux ~~(NPC) accounts for~~results in a mean oxygen loss of 0.03 mol m^{-2} $month^{-1}$ ~~over~~during the mixing period (from October to April) and a gain of 0.06 mol m^{-2} $month^{-1}$ during the stratified period (Fig. S3a). ~~The maximum~~Maximum magnitudes of biological production (> 2 mmol O_2 m^{-2} day^{-1}) are located near the surface during the periods of winter mixing and the associated phytoplankton bloom, ~~and then in the~~ before shifting to subsurface layers later in the year (Fig. ~~6f). The~~S4f). Oxygen consumption ~~is maximum~~peaks in fall between 100 and 200 m depth, and during the mixing period below the mixed layer. During the stratified period, ~~the~~a relatively thick subsurface oxygen maximum (SOM) layer ~~remains~~persists around 70 m depth, ~~above~~overlying the subsurface maximum of biological production located at around 140 m depth, close to the deep chlorophyll maximum (Fig. ~~6b, 6c~~S4b, c, and ~~6f~~f). This is in agreement with the findings of the modelling study of Di Biagio et al. (2022). ~~As for~~In the intermediate layer (150-400 m), ~~it shows~~the ecosystem is characterized by a loss of oxygen throughout the year, with ~~values of~~ biogeochemical ~~flux above -10~~fluxes reaching values lower -5 mmol m^{-2} day^{-1} ~~over the whole year~~ (Fig. 5b).

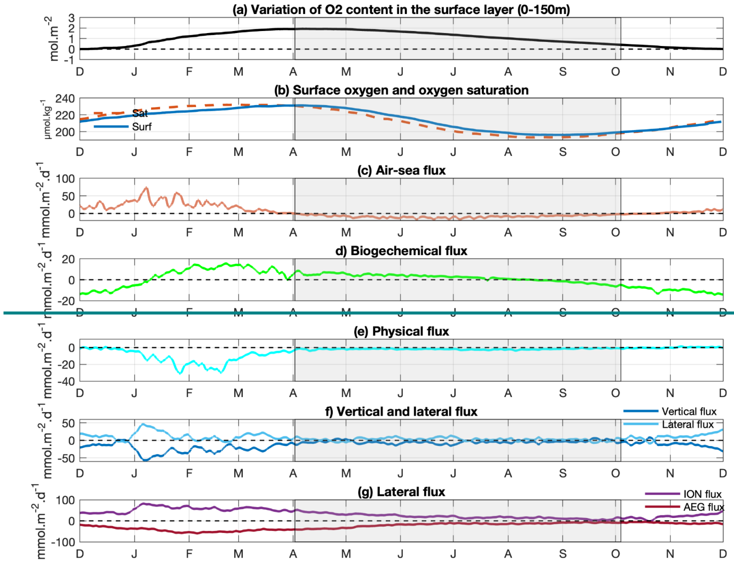

(a) Variation of O2 content in the surface layer (0-150m)
mol.m-2
3
2
1
0
-1
(b) Surface oxygen and oxygen saturation
μmol.kg-1
240
220
200
Sat
Surf
(c) Air-sea flux
mmol.m-2.d-1
100
50
0
d) Biogechemical flux
mmol.m-2.d-1
20
0
-20
(e) Physical flux
mmol.m-2.d-1
0
-20
-40
f) Vertical and lateral flux
Vertical flux
Lateral flux
mmol.m-2.d-1
50
0
-50
(g) Lateral flux
ION flux
AEG flux
mmol.m-2.d-1
100
0
-100
D
J
F
M
A
M
J
J
A
S
O
N
D

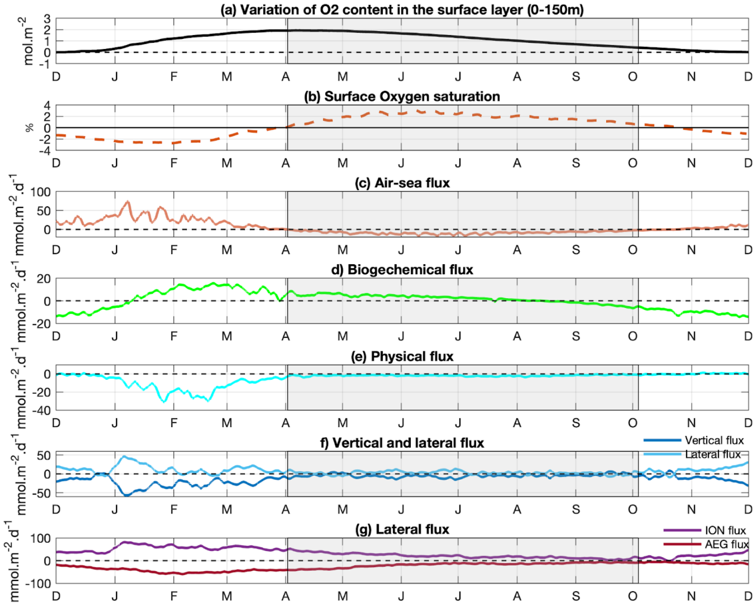

(a) Variation of O2 content in the surface layer (0-150m)
mol.m-2
3
2
1
0
-1
(b) Surface Oxygen saturation
%
4
2
0
-2
-4
(c) Air-sea flux
mmol.m-2.d-1
100
50
0
d) Biogechemical flux
mmol.m-2.d-1
20
0
-20
(e) Physical flux
mmol.m-2.d-1
0
-20
-40
f) Vertical and lateral flux
Vertical flux
Lateral flux
mmol.m-2.d-1
50
0
-50
(g) Lateral flux
ION flux
AEG flux
mmol.m-2.d-1
100
0
-100
D
J
F
M
A
M
J
J
A
S
O
N
D

Figure 4: Oxygen concentration and budget of the 0-150 m layer of the Levantine Basin averaged over the period of study. (a) Variation of the dissolved oxygen inventory (mol m^{-2}) relative to initial conditions (Values are normalized to the starting time point), (b) surface oxygen ~~concentration (blue) and oxygen solubility~~saturation (orange) ~~(µmol O_2 kg^{-1}),~~ = (DOx −DOx sat)/DOx sat ×100%), (c) air-sea flux (positive values correspond to downward fluxes, mmol O_2 m^{-2} day^{-1}), (d) biogeochemical flux (mmol O_2 m^{-2} day^{-1}), (e) sum of vertical (through the 150 m depth) and lateral (exchanges with the Ionian and Aegean Seas) transport fluxes (mmol O_2 m^{-2} day^{-1}), (f) vertical (light blue) and lateral (dark blue) fluxes (mmol O_2 m^{-2} day^{-1}), (g) lateral fluxes at the boundary with the Ionian (purple) and Aegean (red) Seas (mmol O_2 m^{-2} day^{-1}). Horizontal transport fluxes are scaled to the area of the Levantine ~~basin~~Basin for comparison with the other budget terms.The grey shaded area represents the stratification period.

The air-sea oxygen flux displays a marked seasonal pattern (Fig. 4b). During the October-April mixing period, the Levantine Basin, which is undersaturated in oxygen compared to the atmosphere, ~~is~~acts as a sink of atmospheric oxygen. ~~Oxygen~~From September onward, oxygen solubility has increased (Fig. 4b) with the decrease in surface temperature (Fig. 3d) since September. In parallel, the gradual deepening of the mixed layer favors an increase in the surface oxygen concentration, through the mixing of surface O_2 poorer waters with subsurface O_2-rich waters (Fig. ~~6c), which remains lower than~~S4c), although surface concentrations remain below the ~~oxygen at~~ saturation level. The air-sea flux~~,~~, is particularly strong in winter ~~when the~~under strong wind ~~is intense,~~conditions, and reaches maximal values around 70 mmol m^{-2} day^{-1} ~~beginning of~~in early January (Fig. 4c). ~~The air-sea flux~~When averaged ~~during~~over the mixing period, the air-sea flux amounts to 0.50 mol O_2 m^{-2} month^{-1} (Fig. S3a). At the onset of the stratified period (April - May), surface oxygen concentration ~~reaches~~increases to 230 µmol kg^{-1} ~~(Fig. 4b),~~, slightly exceeding saturation levels due to biological oxygen production in the surface layer (Sect. 3.2.4). As a result, the Levantine Basin becomes a source of oxygen for the atmosphere (Fig. 4c). During the rest of the stratified period, the surface oxygen concentration continues to present values higher than the oxygen solubility, leading to continuous outgassing of O_2. We estimate a mean net release of 0.26 mol O_2 m^{-2} month^{-1} of oxygen to the atmosphere over the whole stratified period (Fig. S3a).

Formatted: Font: Gungsuh

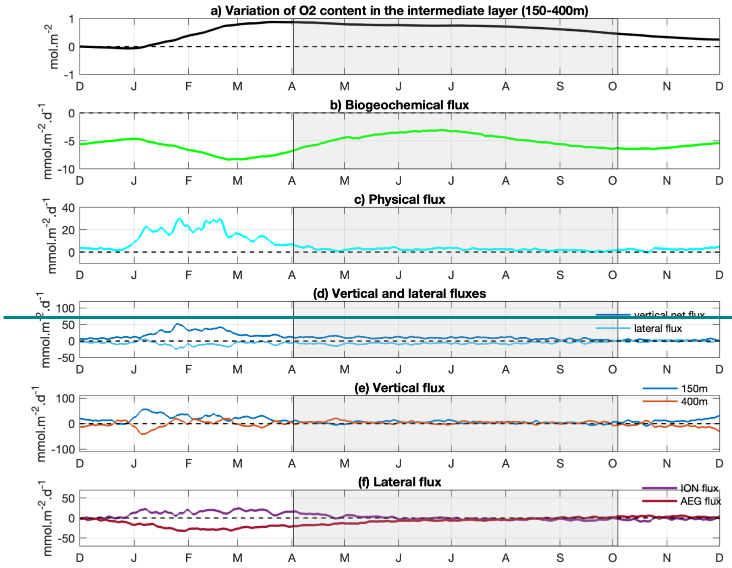
a) Variation of O2 content in the intermediate layer (150-400m)
mol.m-2
1
0
-1
b) Biogeochemical flux
mmol.m-2.d-1
0
-5
-10
c) Physical flux
mmol.m-2.d-1
40
20
0
(d) Vertical and lateral fluxes
mmol.m-2.d-1
100
50
0
-50
vertical net flux
lateral flux
(e) Vertical flux
mmol.m-2.d-1
100
0
-100
150m
400m
(f) Lateral flux
mmol.m-2.d-1
50
0
-50
ION flux
AEG flux
D
J
F
M
A
M
J
J
A
S
O
N
D

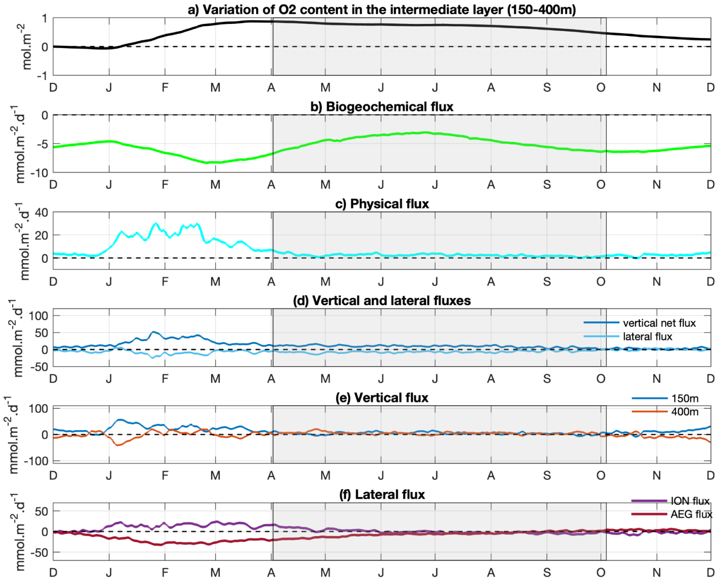

Figure 5: Mean annual cycle of (a) variation of the dissolved oxygen inventory (mol m^{-2}) relative to initial conditions (Values are normalized to the starting time point), and the different oxygen fluxes (mmol m^{-2} day^{-1}): (b) biogeochemical flux, (c) total vertical and horizontal transport, (d) vertical (downward) flux (light blue) and lateral flux (dark blue), (e) the vertical fluxes at 150 and 400m and (f) the lateral Ionian (purple) and Aegean (red) fluxes, in the intermediate layer (150-400 m) and averaged over the Levantine Basin. The grey shaded area represents the stratification period.

Formatted: Font: Bold

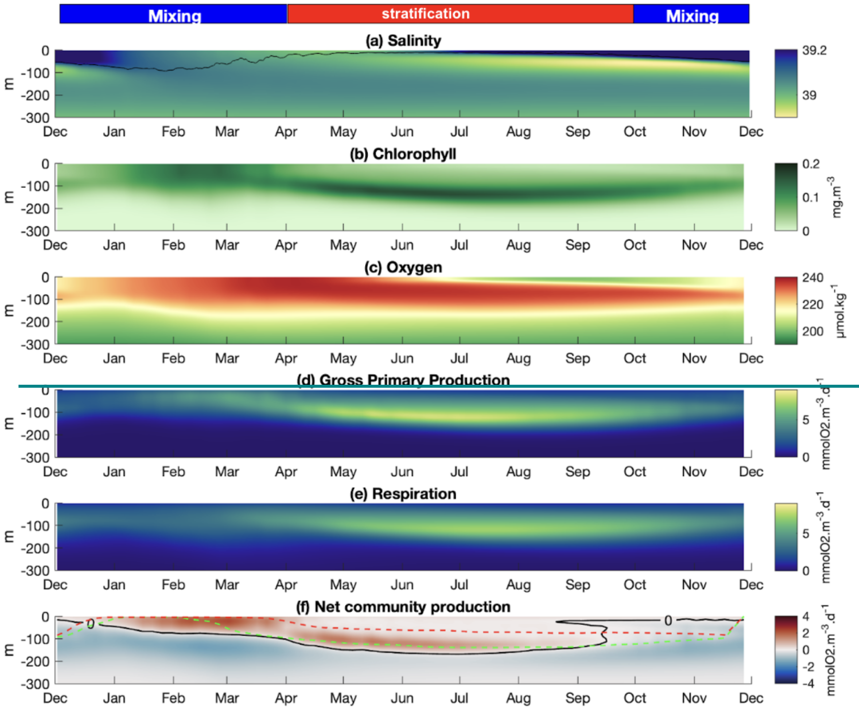

~~Figure 6: Hovmöller diagrams of (a) salinity, (b) chlorophyll (mg m^{-3}), (c) dissolved oxygen concentration (µmol kg^{-1}), (d) gross primary production (mmol m^{-2} day^{-1}), (e) community respiration (mmol m^{-2} day^{-1}), and (f) net community production (mmol m^{-2} day^{-1}), averaged over the Levantine Basin, from December 2013 to May 2021. The black line in (a) indicates the mixed layer depth.~~

~~3.3. Interannual variability~~

~~We investigated~~3.2. Interannual variability

The analysis of the seasonal cycle shows that oxygen fluxes exhibit their largest variability during winter, as reflected by higher standard deviations. In addition, correlations between annual oxygen processes ~~operating at the annual scale~~(NCP, downward export, …) and seasonal fluxes~~, identifying~~ indicate that winter ~~as~~is the most influential ~~period. In~~ season on oxygen dynamics (Fig. S5). Therefore, the following section~~, we therefore focus our analysis~~ focuses on winter~~. For~~ conditions to investigate the ~~purposes~~interannual variability of ~~this study, the year is defined as running from December to the following December.~~

~~3.3.1 Atmospheric forcing and vertical mixing~~

oxygen-related processes. Winter (December-January-February) heat loss ~~exceeded~~exceeds the seasonal mean value of 152 W m^{-2} for years 2014-15, 2016-17, 2018-19, and 2019-20 (Fig. ~~7a~~6a, Table ~~S1~~S2). In contrast, wind stress does not show consistent ~~interseasonal variability~~interannual signals, with peak values around 0.2 N m^{-2} occurring ~~each year~~every winter (Fig. ~~7b~~6b). The ML depth presents interannual variability ~~mostly~~primarily associated with variations in heat loss fluxes (Fig. ~~7a~~6a and ~~7c), with higher values~~6c). ML deeper than the ~~averaged one~~7-year mean value of 108 m are found during the winters 2014-15, 2016-17, and 2018-19 (Table ~~S1~~S2). Based on the mean winter heat flux~~,~~ (W-HF), and mean and maximum ML, the years were classified into two categories: as mild and cold winter years~~: years~~. Years with both winter heat loss and maximum ML above the seven-year means, i.e. 2014-15, 2016-17 and 2018-19, are ~~considered~~ classified as cold winter years~~ while~~, whereas the remaining years, 2013-14, 2015-16, 2017-18 and 2020-21, are ~~considered~~classified as mild years.

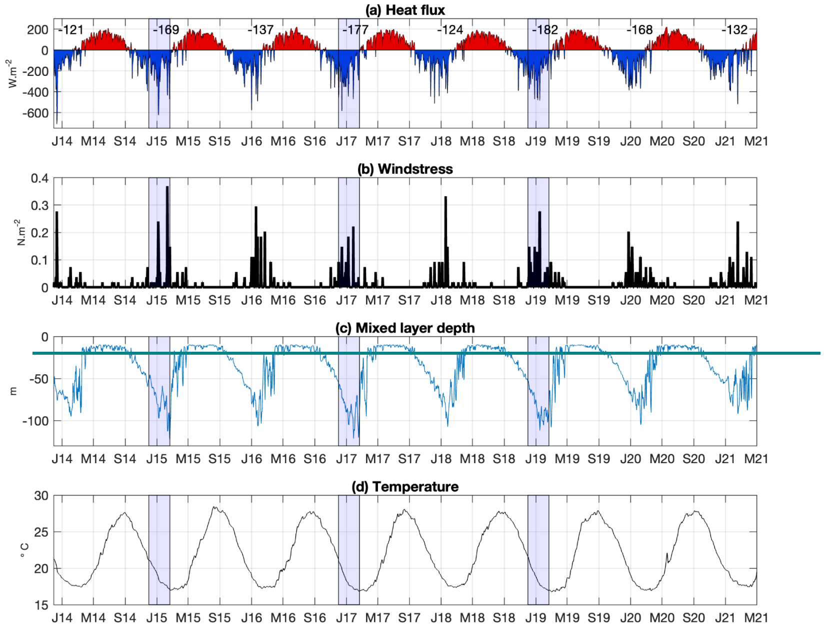

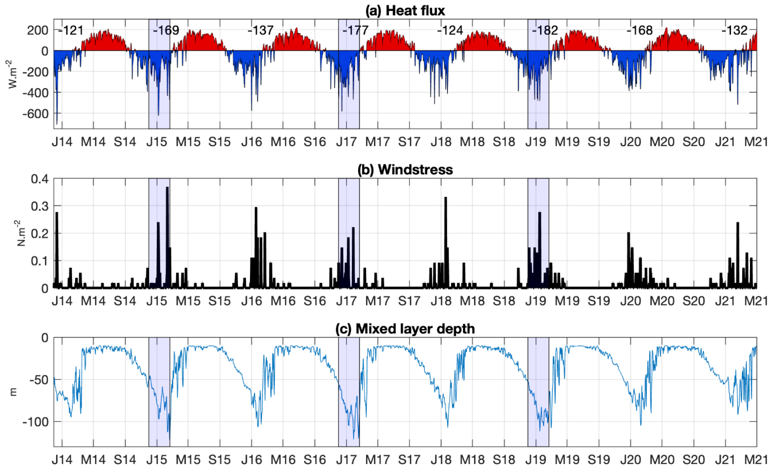

Figure ~~7~~6: Time series of modeled (a) air-sea heat fluxes (W m^{-2}), (b) wind stress (N m^{-2}), and (c) mixed layer depth (m~~)~~), averaged over the Levantine Basin. The mean winter (December-January-February) heat loss is indicated in (a). The blue shaded area represents the winter of the cold winter years.

Formatted: Font: Not Bold

~~3.3.2 Dissolved oxygen fluxes in the surface and intermediate layers~~

All years display qualitatively similar seasonal oxygen cycles in the surface layer (Fig. ~~8~~7). However, ~~colder~~cold winter years (2014–15, 2016–17, 2018–19) exhibit ~~the highest~~substantially larger oxygen fluxes and ~~greater~~stronger inventory variations. ~~In winter,~~ During these winters, changes in oxygen inventory ~~changes~~ exceed 2 mol O_2 m^{-2} (Fig. ~~8a~~ 7a). During phytoplankton blooms in these cold winters, biogeochemical fluxes surpass 20 mmol m^{-2} day^{-1} (Fig. ~~8d~~ 7d). Lateral and vertical transports of dissolved oxygen at the surface layer boundaries ~~show peaks of~~are also enhanced during cold winters. Lateral inflow from the Ionian Sea, lateral outflow toward the Aegean Sea, and downward export to the intermediate layer, show peak values exceeding 100, 75, and 100 mmol m^{-2} day^{-1}, respectively (Fig. ~~8f~~ 7f–g). ~~Air~~In addition, air-sea oxygen fluxes also exceed 150 mmol m^{-2} day^{-1} ~~(~~during cold winters (Fig. ~~8e~~ 7c).

Formatted: Not Superscript/ Subscript

In the intermediate layer, cold winter years ~~also present~~likewise display the ~~highest~~strongest O_2 winter fluxes and the largest oxygen inventory variation compared to mild winter years (Fig. ~~9~~8). Biogeochemical ~~flux exhibits~~fluxes exhibit pronounced negative peaks exceeding -10 mmol m^{-2} day^{-1} during cold winter years (Fig. ~~9b~~8b). While these negative ~~fluxes~~extrema are not significantly stronger than those obtained in ~~warm~~mild years, the subsequent positive fluxes ~~are markedly enhanced~~ following cold winters ~~(less observed~~are markedly enhanced, except during 2016-17~~)~~.. Physical fluxes also are marked by ~~a higher magnitude~~larger magnitudes during cold winters (Fig. ~~9e~~8c-f~~). As found in the upper layer, higher~~), with enhanced lateral and vertical oxygen exchanges~~ occur during~~, as found in the ~~cold winters~~upper layer. Along with the seasonal internal variation, an increasing trend in the inventory is visible from 2013-14 to 2018-19, followed by a decreasing trend until the end of the study period (Fig. ~~9a~~8a).

~~Oxygen fluxes are~~ Overall, oxygen flux variability is partly linked to the variability of winter heat loss (W-HL). ~~There is a~~A strong correlation is found between mean W-HL and winter ~~oxygen~~ downward oxygen export from the surface layer ~~and mean W-HL~~ (R = 0.76, p-value < 0.05, Fig. ~~S4~~S5). Cold years also show ~~high~~enhanced NCP (Net Community Production: gross primary production (GPP) minus community respiration (CR~~)) flux,~~)), with a significant correlation between mean W-HL and annual NCP (R = 0.91, p-value < 0.05, Fig. ~~S4~~S5). When W-HL drops below 135 W m~~$^{-2}$,~~$^{-2}$, the trend suggests a shift of the system ~~shifts~~ from autotrophic to heterotrophic conditions. In the intermediate layer, annual oxygen consumption remains relatively stable but is still significantly correlated with W-HL (R = 0.94, p-value < 0.05). Air-sea oxygen fluxes also show strong correlations with W-HL, both at the annual scale (R = 0.92~~ annually, R = 0.93 in winter~~, p-value < 0.05~~). While~~) and during winter (R = 0.93, p-value < 0.05). Although lateral fluxes ~~increase~~intensify during cold years, only exchanges with the Aegean Sea show a significant correlation with W-HL (R = 0.74 in the surface layer, R = 0.82 in the intermediate layer). ~~The correlation~~Correlations with exchanges from the Ionian Sea ~~is~~are weaker and not statistically significant (R = 0.69, p-value < 0.08).

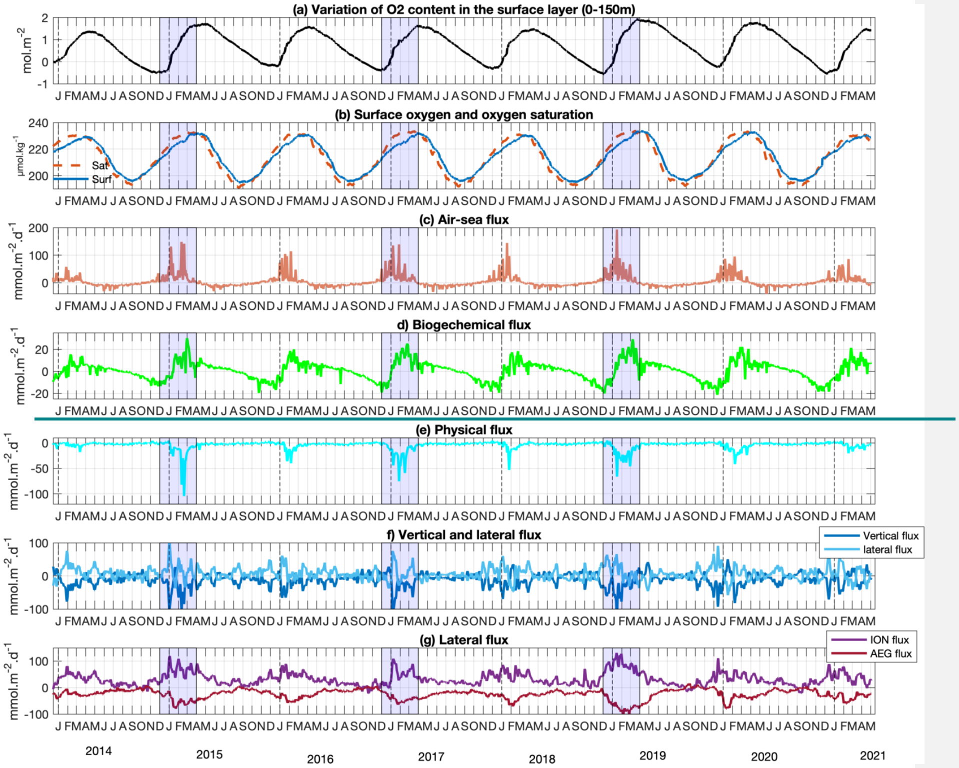

~~**Figure 8: Time series of oxygen concentration and budget of the 0-150 m layer of the Levantine Basin. (a) Variation of the dissolved oxygen inventory (mol m^{-2}) relative to initial conditions (Values are normalized to**~~

~~the starting time point), (b) surface oxygen concentration (blue) and oxygen saturation (orange) (µmol O$_2$ kg^{-1}), (c) air-to-sea flux (mmol O$_2$ m^{-2} day^{-1}), (d) biogeochemical flux (mmol O$_2$ m^{-2} day^{-1}), (e) sum of vertical (through the 150 m depth) and lateral (exchanges with the Ionian and Aegean Seas) transport fluxes (mmol O$_2$ m^{-2} day^{-1}), (f) vertical (light blue), lateral (dark blue) flux (mmol O$_2$ m^{-2} day^{-1}), (g) detailed lateral flux at the boundary with the Ionian (purple) and Aegean (red) seas (mmol O$_2$ m^{-2} day^{-1}). Horizontal transport fluxes are scaled to the area of the Levantine Basin for comparison with the other budget terms. The blue shaded area represents the winter of the cold winter years.~~

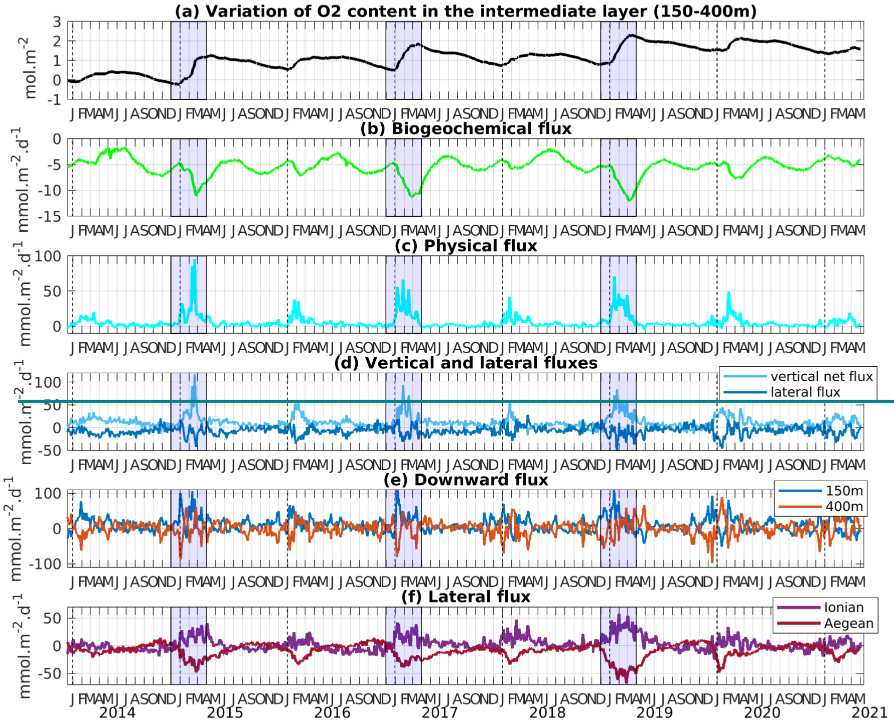

~~Figure 9: Time series of (a) variation of the dissolved oxygen inventory (mol m^{-2}), (b) biogeochemical flux, (c) total vertical and horizontal transport, (d) vertical (light blue) and lateral flux (dark blue), and (g) lateral fluxes from Ionian (purple) and Aegean (red) sea, in the intermediate layer (150-400 m) and averaged over the~~

~~Levantine Basin. The flux unit is mmol m^{-2} day^{-1}.~~

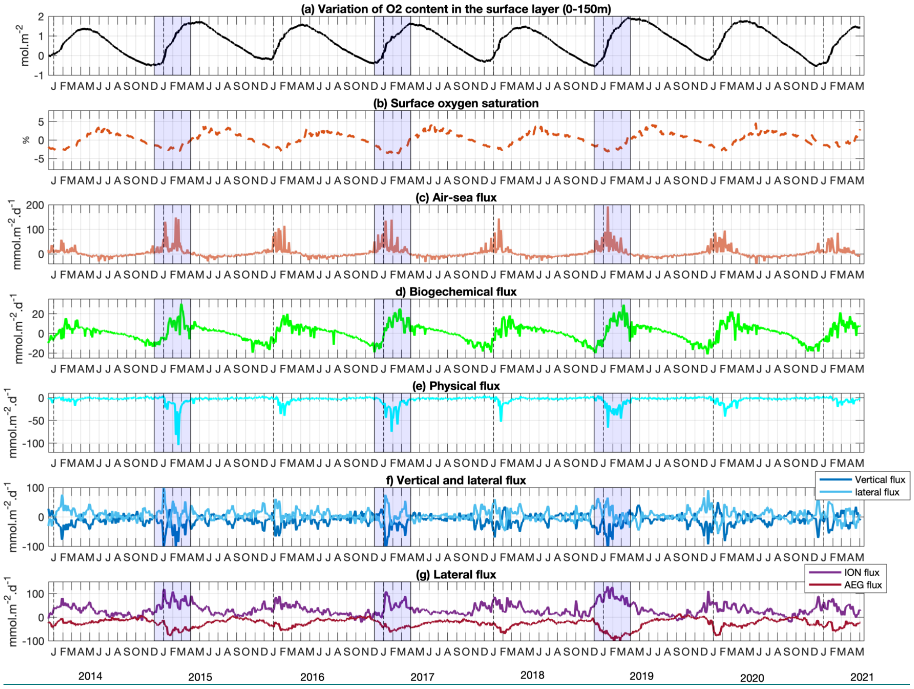

Figure 7: As in Figure 4, but showing the interannual variability of oxygen inventory and budget components for the 0–150 m layer of the Levantine Basin. Blue shading marks cold winters.

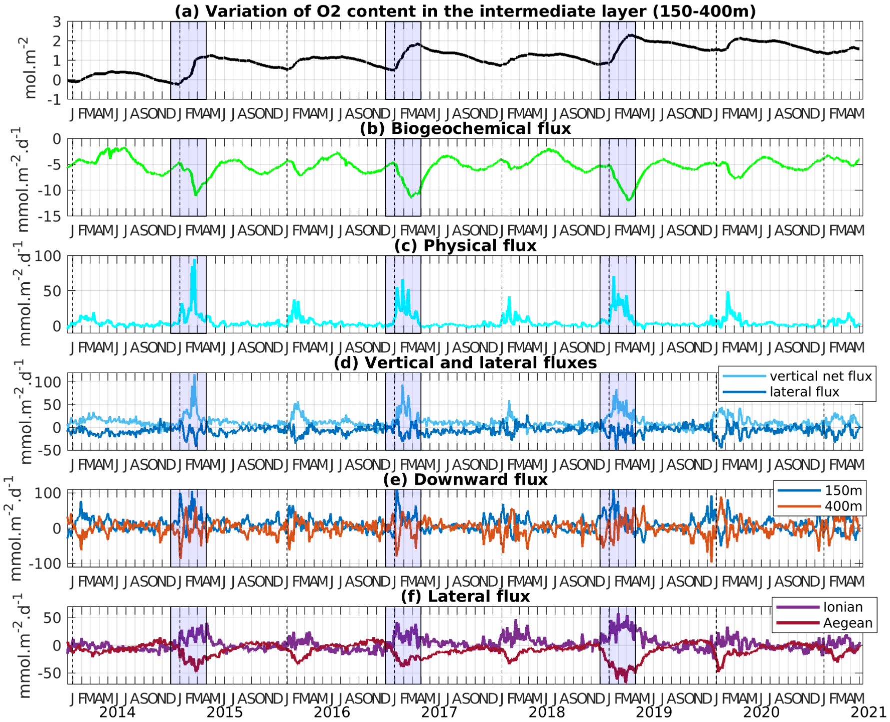

Figure 8: As in Figure 5, but showing the interannual variability of oxygen inventory and budget components for the 150-400 m layer of the Levantine Basin. The blue shaded area represents the winter of the cold winter years.

Formatted: Font: Bold

3.~~4~~3 Annual oxygen budget in the surface and intermediate layers

On an annual basis and ~~on average~~averaged over the seven studied years (Fig. ~~10), the surface layer gains oxygen through air-sea exchange. Additionally, oxygen is transported from the Ionian Sea to the Aegean Sea through both surface and intermediate layers. A fraction of this oxygen is exported to intermediate depths, where it is partially consumed before the remainder reaches the Aegean (Fig. 10). The surface~~ 9), the surface ecosystem of the ~~basin appears to be~~ Levantine Basin generally ~~productive in oxygen. The net biogeochemical~~ acts as a net source of oxygen, although the magnitude and even the sign of the biogeochemical contribution vary substantially from year to year. The surface layer of the basin also exhibits a net gain of oxygen through air-sea exchange. This atmospheric input results from the seasonal alternation between wintertime uptake and summertime outgassing described in Sect. 3.1. In addition to the important air-sea fluxes, the basin receives a significant lateral supply of oxygen through the advection of waters originating from the Ionian Sea into the surface layer. A fraction of the oxygen supplied to the surface is exported downward toward intermediate depths, partially consumed by biogeochemical processes, while a remaining fraction is transported toward the Aegean Sea. On average, the oxygen budget indicates that the net biogeochemical oxygen flux is one order of magnitude smaller than the contributions from transport and air-sea ~~flux, changing sign depending on the considered year, with a strong interannual variability. On average, the~~ exchange.

In the intermediate layer ~~loses~~, the oxygen loss due to biogeochemical consumption ~~but gains it through net~~is compensated by transport, at the annual scale (Fig. ~~10~~9). The physical supply ~~of oxygen comes~~to the intermediate layer arises from both downward ~~inflow~~transport from the surface layer and lateral inflow from the Ionian Sea~~, while part~~. A fraction of ~~the~~ oxygen in intermediate waters is also exported toward the Aegean Sea (Fig. ~~10~~9).

Formatted: Font colour: Auto

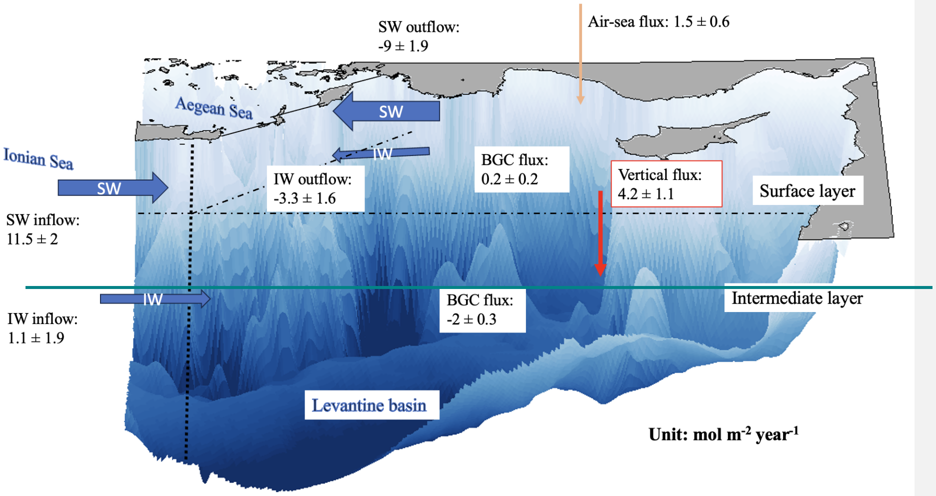

One can notice that in the surface layer, the lateral export of oxygen towards the Aegean Sea is smaller than the net input from the Ionian Sea, and on the contrary, in the intermediate layer, the lateral oxygen export toward the Aegean Sea is larger than the input from the Ionian Sea. This reflects both a small biological production in the surface layer and a large supply of oxygen from the surface layer into the intermediate waters through vertical transfer, occurring mostly during winter mixing, convection and subduction in the Levantine Sea. This budget highlights the role of the Levantine Basin as both a regional sink for intermediate waters and a transit zone for dissolved oxygen within the eastern Mediterranean circulation.

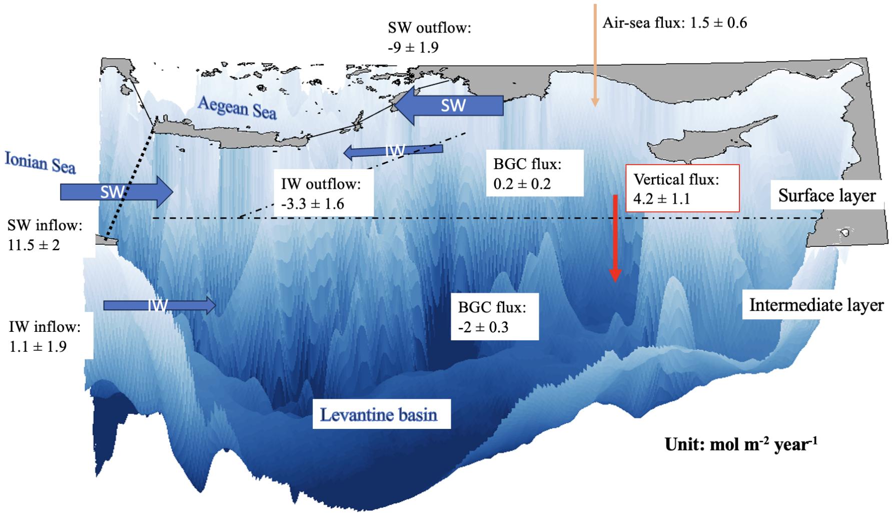

Figure ~~10~~9: Schematic showing the terms of the mean annual oxygen budget (in mol O_2 m^{-2} yr^{-1}) for the Levantine Basin over the period from December 2013 to ~~November~~December 2020. The terms of the budget are estimated for the upper ~~layer~~ (surface-150 m~~),~~) and ~~the~~ intermediate ~~layer~~ (150-400 m~~).~~) layers. SW: surface layer, IW: intermediate layer~~. Arrow thickness is proportional to the intensity of the flow~~.

Formatted: Indent: Left: 0 cm

3.~~5~~4 Spatial variability of oxygen fluxes in the Levantine Basin

At the annual scale, the whole Levantine Basin appears as an atmospheric sink for oxygen, except in the coastal area influenced by the Nile River (Fig. ~~11a). The highest uptake rates in~~ 10a). In the offshore region, the strongest oxygen uptake rates are ~~located~~found in the Rhodes Gyre area, covering 5% of the surface of the Levantine Basin, ~~and~~but contributing 14% of the annual atmospheric oxygen intake. ~~Other~~Additional regions ~~characterized by higher~~ of enhanced uptake rates are located in the North, in the Antalya Bay and the Cilician ~~basin. The~~ Basin identified as another LIW formation area (Fach et al. 2021). The spatial distribution of the annual air-sea oxygen flux is ~~also spatially mostly~~largely controlled by the winter air-sea O_2 flux (not shown). The annual anomalies show that ~~the~~ cold years (2014-15, 2016-17 and 2018-19) ~~absorb more~~are associated with enhanced atmospheric oxygen ~~in~~uptake over the ~~whole sea~~entire basin (Table ~~S2~~S3), and especially in the Rhodes Gyre (Fig. ~~S7~~S8). In this main area of intermediate water formation, the vertical mixing period is characterized by the upward supply of ~~cold~~colder and oxygen-poorer water from ~~the~~ intermediate ~~layer towards~~depths to the surface~~ during the winter mixing period is~~, more pronounced than in surrounding areas. ~~Thus, the~~The resulting negative temperature and oxygen anomaly~~, as well as the negative oxygen anomaly, enhanced the~~ reinforce surface undersaturation in this area~~ that shows~~, reaching maximum values varying between 2 and 5 % (with higher values during cold winter years). In contrast to the ~~entire~~ basin-wide functioning, where oxygen is generally exported downward from surface to intermediate layers, the ~~model indicates that the~~ Rhodes Gyre ~~displayed~~displays an inverse pattern~~, with~~. In this area, oxygen is transported upward from intermediate depths ~~to~~toward the surface, ~~balanced by a lateral export~~and subsequently redistributed laterally. This lateral transfer is particularly strong ~~in~~during winter and ~~takes place notably through~~is associated with the dispersal of LIW by subduction (Estournel et al., 2021~~). The model~~).

Model results also show a marked spatial heterogeneity ~~of~~in the balance between GPP and CR, expressed through net community production (NCP), when averaged ~~along~~over the period of study in the surface layer (surface-150 m~~) (~~; Fig. ~~11b~~10b). Positive NCP values are found in a central ~~area including~~region encompassing the cyclonic Rhodes Gyre and other cyclonic gyres (e.g., West Cyprus gyres~~,...), and~~), as well as in the coastal areas influenced by ~~rivers~~river inputs. In particular, the Rhodes Gyre contributes to 41% of the total annual biological oxygen production in the surface layer of the ~~whole~~entire basin. ~~NCP is~~In contrast, negative values of NCP prevail in the along-slope circulation, and ~~in~~within the anticyclonic Mersa-Matruh Eddies and Shikmona Eddy. ~~It~~Annual NCP follows the same spatial pattern throughout all the years with a more ~~accentuated~~pronounced production in the cyclonic gyres during cold years compared to ~~the~~ mild ~~years~~winters (Fig. ~~S6).~~

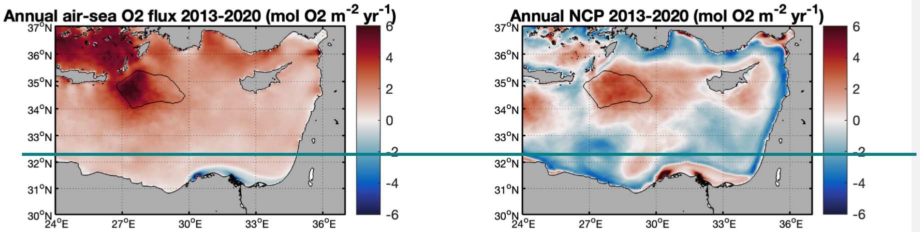

S7).

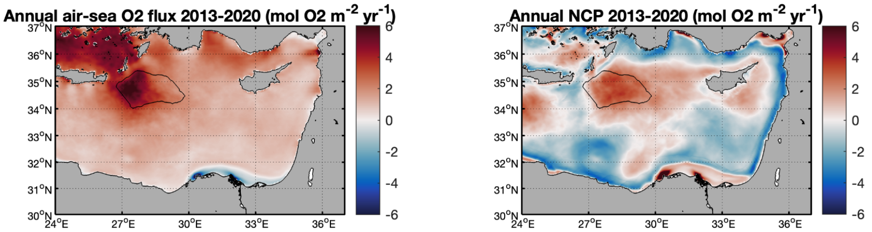

Figure ~~11~~10: Modeled annual air-sea oxygen flux and net community production (NCP, mol O_2 m^{-2} yr^{-1}) in the surface layer (0-150 m) for the period from December 2013 to December 2020. The black line delimits the Rhodes ~~gyre.~~Gyre. Positive values for the air-sea oxygen flux indicate a net flux of oxygen into the ocean (uptake), while negative values indicate a net flux from the ocean to the atmosphere. Positive NCP values correspond to net biological oxygen production and negative values to consumption.”

Formatted: Font: Not Bold

4 Discussion

In the present study, we ~~have~~ used a 3D coupled physical-biogeochemical model to investigate the dynamics of oxygen in the Levantine Basin. The physical and biogeochemical parts of the coupled model were previously validated by Estournel et al. (2021) and Habib et al. (2023), respectively. Here we have further compared our results on the oxygen cycle with two types of in situ ~~data~~observations: high-resolution BGC-Argo data and data from research cruises. The major limitation highlighted by these comparisons is the representation of the subsurface oxygen maximum layer. The ~~observed~~marked heterogeneity of this layer in observations, with ~~a~~ maximum ~~concentration~~concentrations in ~~the~~its upper part ~~and then~~followed by a progressive decrease of its value ~~further deeper~~with depth, is not ~~well~~fully reproduced in the model. The increase of the maximum value during the summer period, shown in the BGC-Argo data, ~~could be attributed to~~may reflect production or respiration processes~~,~~ that are underestimated or overestimated, respectively, in the model. ~~This~~Alternatively, this discrepancy ~~could also~~may be explained by physical processes with a misrepresentation of the thickness of the subsurface oxygen maximum layer in the model. In that case, a finer vertical resolution at those depths or an improvement of the vertical advection scheme, avoiding possible spurious numerical mixing, as proposed by Garinet et al. (2024), could be tested in future works to reduce ~~the~~ potential excessive vertical diffusivity.

Formatted: Font: Not Italic

Our budget of oxygen is subject to sources of uncertainties linked to the physical and biogeochemical models used in this study. One approach to overcome single-model uncertainties and limitations would be to adopt a multi-model approach. An alternative approach would consist in estimating oxygen budgets using observational syntheses; however, the sparse spatial coverage of in situ data currently limits the closure of basin-scale oxygen budgets based solely on observations. Finally, a complementary strategy could involve a combined approach such as that developed by Di Biagio et al. (2023) which relies on biogeochemical reanalysis corrected with Argo float data. Despite ~~this limitation,~~these limitations linked to the models used here, we found that the seasonal variations of oxygen solubility and concentration align with previous observational studies ~~(Kress and Herut, 2001; Schlitzer et al., 1991) and we used the model to estimate~~(Kress and Herut, 2001; Schlitzer et al., 1991). To provide a first quantitative assessment of the contribution of various processes—air-sea flux, physical dynamics, and biogeochemical processes—to oxygen ~~dynamics and the overall budget~~budget, we chose an online and strictly closed budget approach. As shown by Trinh et al. (2024), this approach can yield substantially higher accuracy than offline calculations, especially in the quantification of lateral fluxes.

The model shows a net annual weak biological production of oxygen in the surface layer of the Levantine Basin, primarily due to the sea's oligotrophic nature, which is more pronounced in the southeastern regions of the Levantine Basin (D'Ortenzio, 2009; Lavigne et al., 2015). This oligotrophy is attributed to an anti-estuarine circulation characterized by an eastward inflow of surface nutrient-depleted waters and an outflow of intermediate nutrient-rich waters resulting from the water formation (Robinson and Golnaraghi, 1993). Interannual variability is nevertheless observed here, with the sea being heterotrophic during ~~warm~~mild winter years (2014 and 2018~~ here), as detected~~), consistent with the findings by Mayot et al. (2016) using satellite ocean color data. By considering both surface and intermediate layers, the Levantine Sea appears as a net heterotrophic system in the model results. This ~~aligns~~is in line with ~~the review by Siokou-Frangou et al. (2010) and the study by Christaki et al. (2011), depicting a large~~previous studies reporting strong temporal and spatial heterogeneity in the trophic status of the oligotrophic Levantine Basin~~.~~ (Christaki et al., 2011; Siokou-Frangou et al., 2010). The planktonic ecosystem ~~in the Levantine Basin is strongly~~is largely regulated by ~~the basin's~~ heterotrophic ~~component. Siokou-Frangou et al. (2002) observed an increase in the~~ processes, with higher heterotrophic/autotrophic biomass ~~ratio with higher values more frequently found~~ratios typically observed in the most oligotrophic regions and during ~~the~~ stratified ~~period. This pattern aligns with the spatial trend reported by Christaki et al. (2002), who depicted a longitudinal increase in this ratio from the Balearic Sea to the eastern Levantine Sea.~~periods (Christaki et al., 2002; Siokou-Frangou et al., 2002). Despite this general heterotrophic ~~system, highly dynamic~~character, mesoscale physical structures ~~favoring deep~~promoting vertical mixing~~,~~ and ~~in particular~~ nutrient upwelling~~, determine the~~ play a key role in shaping the basin's trophic ~~gradient of the Levantine Basin (Siokou-Frangou et al., 2010), varying from marked recycled production to new production systems (Legendre and Rassoulzadegan, 1995). This variability was also detected in nutrient concentrations from different parts of the Levantine Basin. A shallow nutricline, coupled with an upward nutrient flux, was found in~~gradients, particularly within cyclonic systems~~, whereas the opposite effect occurred in anticyclonic systems (Salihoğlu et al., 1990)~~ (Legendre and Rassoulzadegan, 1995; Salihoğlu et al., 1990). ~~This pattern was also reflected in the spatial distribution of chlorophyll.~~ Our model results show the high contribution of the Rhodes Gyre to the annual oxygen biological production in the surface layer of the whole Levantine Basin area (around 41%). ~~In the intermediate layer, biogeochemical fluxes~~It has been identified as the major area of LIW formation, characterising winter vertical mixing enriching the surface layer with nutrients and stimulating primary production (D'Ortenzio et al., 2021; Lavigne et al., 2013). In the intermediate layer, biogeochemical fluxes in the Gyre and the Levantine Basin exhibit little variation between mixing and stratification periods, especially during cold years, consistent with the findings of Roether and Well (2001) and Klein et al~~.,~~. (2003).

Commented [1]: dans l'étude citée ou dans le modèle?

The model indicates that the Levantine Basin absorbs atmospheric oxygen from November to April, while releasing it during the rest of the year. This is in line with ~~the~~previous observational and modelling studies ~~of (~~(Schlitzer et al. ~~(~~1991~~)~~, Kress and Herut, ~~(~~2001~~), and~~ ,Di Biagio et al. ~~(~~2022~~). The whole Levantine Basin, except~~). Except for the river-influenced areas (Nile river), ~~shows~~the whole Levantine Basin acts as an annual sink of atmospheric ~~uptake~~oxygen for all studied years~~ (~~, with an average uptake of 1.5 ± 0.6 mol O_2 m^{-2} yr^{-1}~~), with~~, and higher values during cold winter years. ~~The uptake~~Uptake is enhanced in intermediate water formation areas, in particular in the Rhodes Gyre, where ~~the~~ undersaturation ~~is increased~~increases during ~~the~~ winter ~~period, when~~due to stronger surface cooling and mixing of poorer O_2 water masses~~ are mixed~~ with surface waters, in agreement with what was previously observed and modeled in other water formation areas (Copin-Montégut and Bégovic, 2002; Coppola et al., 2017, 2018; Di Biagio et al., 2022; Fourrier et al., 2022; Körtzinger et al., 2004, 2008; Ulses et al., 2021; Wolf et al., 2018). The Rhodes Gyre shows a comparable winter uptake rate (20.3 ± 7.4 mol O_2 m^{-2} yr^{-1}) as other water formation areas such as the Labrador Sea and Gulf of Lion (ranging between 11 and 37 mol m^{-2} yr^{-1}; Copin-Montégut & Bégovic, 2002; Coppola et al., 2017, 2018; Körtzinger et al., 2008; Ulses et al., 2021; Wolf et al., 2018). As a matter of comparison, the 7-year averaged oxygen uptake estimated here for the whole Levantine Basin, characterized by relatively low solubility compared to the rest of the Mediterranean (Mavropoulou et al., 2020, Di Biagio et al., 2022), represents 64% of the oxygen uptake by the NW Mediterranean deep convection estimated for the cold year 2012-13 with the same coupled model (Ulses et al., 2021). These estimates are nevertheless subject to methodological uncertainties. In particular, air–sea oxygen fluxes depend on the parameterization of the gas transfer velocity, whose sensitivity to wind speed and formulation can induce uncertainties of the order of 12-16%, as quantified by Ulses et al. (2021). Additional uncertainties arise from surface heat flux estimates and the representation of vertical mixing, but these are not expected to modify the relative importance or seasonal phasing of the dominant budget terms (Josey et al., 2013; Large et al., 1994).

Regarding ~~the oxygen~~ vertical oxygen transport in the whole Levantine Basin, the weak upward transfer from the deep layer into the intermediate layer found in our results is consistent with the general scheme of circulation or oxygen cycle shown in previous studies (Mavropoulou et al., 2020; Powley et al., 2016; Roether and Schlitzer, 1991; Tanhua et al., 2013) describing a gradual upwelling of deep water originating from the Adriatic Sea or Aegean Sea. While a downward export of oxygen from the surface layer to the intermediate layer is simulated at the scale of the whole basin, the Rhodes Gyre exhibits an opposite pattern, with oxygen being transported upward from the intermediate layers to the surface. This upward input ~~in~~into the surface layer is balanced by a lateral export, particularly strong in winter, which takes place notably through the dispersal by subduction of the newly formed LIW ~~as~~at the periphery of the mixed patch, which is consistent with the observations reported by Malanotte-Rizzoli et al. (2003) for January 1995 during the POEM cruise~~.~~ and by Taillandier et al. (2022) during PERLE cruises.

~~Our~~Finally, our results on lateral oxygen exchanges are also in agreement with previous studies describing the general circulation in the ~~eastern Mediterranean Sea. Regarding the exchanges with the Aegean Sea, a net outflow of LSW and LIW by the Asia Minor Current through the Cretan Straits was documented in several observational and modeling studies (Estournel et al., 2021; Millot and Taupier-Letage, 2005; Theocharis et al., 1993; Velaoras et al., 2014; Zodiatis, 1993).~~Eastern Mediterranean Sea under BIOS cyclonic phases. During these cyclonic phases of the BIOS, the cyclonic Northern Ionian Gyre promotes an important eastward advection of Atlantic Water toward the Levantine Basin. As for the exchanges with the Ionian Sea, the general cyclonic circulation displays in the surface and intermediate layers an eastward inflow along the Libyan-Egyptian coast (Estournel et al., 2021). South of Crete, the flux reverses seasonally with an inflow from the Ionian in winter and an outflow in summer (Estournel et al., 2021). The net oxygen flux directed from the Ionian toward the Levantine Basin in surface and intermediate waters in this study results from a stronger southern input than the northern export at the Ionian-Levantine boundary. Regarding the exchanges with the Aegean Sea, a net outflow of LSW and LIW by the Asia Minor Current through the Cretan Straits was documented in several observational and modeling studies (Estournel et al., 2021; Millot and Taupier-Letage, 2005; Velaoras et al., 2014). During anticyclonic phases of the BIOS, the inflow from the Ionian Sea of Atlantic Water is reduced and significant changes in oxygen circulation may be expected and deserve further investigation.

In addition, extreme events may episodically modulate air–sea oxygen exchanges in the Levantine Basin. In particular, marine heatwaves, whose frequency and intensity have increased in the Eastern Mediterranean in recent decades (Aboelkhair et al., 2023; Darmaraki et al., 2024), can enhance upper-ocean stratification, reduce vertical ventilation, and decrease oxygen solubility through surface warming, potentially leading to transient oxygen anomalies in the upper and intermediate layers (Keeling et al., 2010; Schmidtko et al., 2017). Moreover, Medicanes, short-lived and spatially localized extreme events, could also impact biological dynamics and air-sea exchanges on their passage (Menna et al., 2023; Jangir et al., 2024; Jangir et al., 2026; Reale et al., 2026). While a dedicated analysis of the impacts of those extreme events (marine heatwaves, Medicanes) is beyond the scope of the present study, their effects may contribute to short-term departures from the mean seasonal oxygen cycle and their integrated contribution to basin-scale and annual oxygen budget .will need to be assessed in future works.

Beyond the Levantine Basin, the processes identified here have broader implications for regional biogeochemical dynamics and Earth system modelling. The quantified oxygen budget of LIW highlights the sensitivity of intermediate-water ventilation to circulation and atmospheric forcing at seasonal to interannual timescales in semi-enclosed basins (e.g. Tanhua et al., 2013; Schneider et al., 2014). Because LIW supplies the Eastern Intermediate Water and flows in the whole Mediterranean basin, variability in its oxygen content may propagate in the other water formation areas (South Aegean, South Adriatic, north-western Mediterranean), and as it constitutes the main precursor of the Mediterranean Overflow Water, can influence the oxygen and biogeochemical properties of intermediate waters beyond the Mediterranean in the Northeast Atlantic (Aldama-Campino & Döös, 2020; Stendardo and Gruber, 2012). Accurately representing these processes is therefore essential for regional biogeochemical models and Earth system models aiming to capture Mediterranean–Atlantic exchanges and their contribution to large-scale oxygen budgets.

5 Conclusion and future works

The study period was marked by contrasted atmospheric and hydrodynamic winter conditions. The confrontation of the model results with cruise and BGC-Argo float observations shows the capacity of the model to capture the general seasonal and spatial dissolved oxygen variability~~ and~~, as well as the main oxygen features in the ~~basin~~Levantine Basin. These in situ observations, particularly from BGC-Argo floats and ship-based measurements, were essential ~~in~~for constraining and validating the simulations, without which the model outputs would not have reached their current level of reliability. The following conclusions can be drawn:

- The model results indicate a clear seasonal cycle for the oxygen air-sea flux. During winter, with the decrease in temperature, the increase in heat losses and intensified vertical mixing events, the surface layer is undersaturated in oxygen~~ and thus absorbs~~, resulting in atmospheric oxygen ~~at the surface. The undersaturation~~uptake. Undersaturation averaged over the whole basin reaches 2 % during winter. During the stratified period, primary production combined with the decrease of the temperature-dependent solubility in the ~~surface~~thin mixed layer above the SOM leads to oxygen oversaturation and subsequent outgassing~~, with a maximum oversaturation of 0.6% observed in summer~~.

- ~~The~~ At the annual scale, the Levantine Basin acts as a net sink for ~~the~~ atmospheric oxygen~~ at an annual scale,~~ , capturing 1.5 ± 0.6 mol O_2 m^{-2} yr^{-1} of oxygen. Most of the oxygen uptake occurs during winter, when it accounts for 10.7 ± 2.8 mol O_2 m^{-2} yr^{-1}. The Rhodes Gyre absorbs atmospheric oxygen at a 2-fold higher rate than the ~~whole~~entire Levantine Basin.

- Our budget shows that the surface layer of the Levantine Basin is a net source of dissolved oxygen for the intermediate ~~depths~~waters, with winter vertical export of oxygen ~~influenced~~strongly modulated by the winter heat loss intensity. Regarding the exchanges with the surrounding seas, we found that oxygen is laterally transported into the Levantine Basin by surface and intermediate waters originating from the Ionian Sea~~ into the basin, and from the basin towards the Aegean Sea.~~. The lateral annual oxygen outflow ~~to~~toward the Aegean Sea is strongly enhanced by the heat loss intensity with exports 1.5 and 2.4 times higher during cold years in the surface and intermediate layer, respectively, compared to mild years.

- ~~The~~On an annual level, the Levantine Basin is found to act as a weak autotrophic ecosystem~~ on an annual level~~, with a net community production in the surface layer alternating between auto- and heterotrophic status

Formatted: Outline numbered + Level: 1 + Numbering Style: Bullet + Aligned at: 0,63 cm + Indent at: 1,27 cm influenced by the magnitude of the winter heat loss. In deeper depths~~,~~ and respiration ~~and nitrification~~ resulted in an oxygen consumption of 2.0 ± 0.3 mol O_2 m^{-2} yr^{-1}. Spatially, the Rhodes Gyre appears to be a major oxygen reservoir across the basin, contributing 41% of the oxygen production of the whole surface layer.

This ~~work~~study represents a first step in our modeling of the dissolved oxygen dynamics in the Levantine Basin. While the quasi-permanent Rhodes Gyre dominates the basin-scale oxygen budget, transient cyclonic and anticyclonic mesoscale structures are also expected to contribute to oxygen variability outside this gyre on shorter time scales, in particular through nutrient upwelling or transport from nutrient-rich coastal waters offshore (Di Biagio et al., 2022; Pirro et al., 2024). Further investigations focusing on the specific role of ~~the~~these various cyclonic and anticyclonic eddies will be conducted in the future. ~~Besides, several~~Future work could also benefit from applying variability-based approaches, such as empirical orthogonal function (EOF) or regime-oriented analyses on model fields, to further disentangle the respective roles of physical and biogeochemical drivers across temporal scales (Di Biagio et al., 2023).

While the 7-year study period provides high-resolution insights into oxygen dynamics, it does not cover long-term climate shifts such as the EMT. Several studies suggest a decadal variability of dissolved oxygen across the whole water column linked to the dense water formations in the south Adriatic and Aegean seas and to the general eastern Mediterranean circulation, notably the reversal of the North Ionian Gyre (Ozer et al., 2020, 2022). ~~A time-extended~~ Extended the simulation ~~of the coupled model~~period, in addition to the implementation of a finer vertical resolution at key depths~~,~~ could contribute to examining this longer-term variability in the Levantine Basin and the connections between the sub-basins of the eastern Mediterranean. Improving the representation of intermediate water oxygen dynamics in the Mediterranean is also a necessary step toward better quantifying Mediterranean–Atlantic biogeochemical coupling and its sensitivity to future climate-driven changes in ventilation and circulation.

Formatted: Highlight

In memoriam

The authors wish to pay tribute to the memory of Pascal Conan, who passed away on August 5, 2025. He made insightful contributions and was unwaveringly dedicated to biogeochemical oceanography. We will greatly miss him both professionally and personally.

Code availability

The SYMPHONIE model and the MATLAB codes used to process the model outputs are available from the authors on request.

Data availability

Data used to validate the model are available on different websites specified in the main text of the paper. These data and the model outputs are also available from the authors on request.

Author contributions

CU, CE, and JH conceptualized the study. CE and PM ran the SYMPHONIE model. PM added the budget calculation to the coupled model. CU and JH calibrated and ran the coupled physical–biogeochemical model. CE validated the physical model, JH the biogeochemical model. Observational data were provided by PC, MPP, MaF, LC, CWR, DL and TM. Funding acquisition was done by MiF, CU and CE. JH, CU, and CE wrote the initial version of the paper. All authors contributed to the revision of the paper and approved the submitted version.

Acknowledgements

This study is a contribution to the MerMex (Marine Ecosystem Response in the Mediterranean Experiment) project of the MISTRALS international program. The numerical simulations were performed using the SYMPHONIE model, developed by the Community Code SIROCCO (https://sirocco.obs-mip.fr/) coordinated by the Research Infrastructure ILICO (CNRS-IFREMER) dedicated to coastal ocean observations (https://www.ir-ilico.fr/?PagePrincipale, last access: 16 June 2025), and computed on the cluster of LAERO/OMP and HPC resources from CALMIP grants (P1331). We acknowledge the scientists and crews of the Flotte océanographique française (https://www.flotteoceanographique.fr/), who contributed to the cruises carried out in the framework of the PERLE project. We thank Franck Dumas, chief scientist of the PERLE 1 campaign, for his role in organizing and leading the cruise. The authors would like to acknowledge the National Council for Scientific Research of Lebanon (CNRS-L), Campus France, the University of Toulouse, and LEGOS for granting a doctoral fellowship to Joelle Habib. We thank Marta Álvarez (IEO, La Coruña) and collaborators for making the CARIMED database available to us.

Formatted: No underline, Font colour: Auto

Financial support

This research has been supported by the international programme MISTRALS (Marine Ecosystem Response in the Mediterranean Experiment – MerMex; https://www.odatis-ocean.fr/activites/activites-liees-au-pole/chantiers/mistrals, last access: 18 August 2025). The numerical simulations were performed with the SYMPHONIE model developed by the Community Code SIROCCO (https://sirocco.obs-mip.fr/) and coordinated by the Research Infrastructure ILICO (CNRS–IFREMER; https://www.ir-ilico.fr/?PagePrincipale, last access: 18 August 2025), with computational resources provided by the cluster of LAERO/OMP and CALMIP grants (P1331). The study also received support from the National Council for Scientific Research of Lebanon (CNRS-L), Campus France, the University of Toulouse, and LEGOS through a doctoral fellowship granted to Joelle Habib.

Formatted: No underline, Font colour: Auto

Formatted: No underline, Font colour: Auto

Formatted: No underline, Font colour: Auto

References

Aboelkhair, H., Mohamed, B., Morsy, M., and Nagy, H.: Co-occurrence of atmospheric and oceanic heatwaves in the Eastern Mediterranean over the last four decades, Remote Sens., 15, 1841, https://doi.org/10.3390/rs15071841, 2023.

Aldama-Campino, A., and Döös, K.: Mediterranean overflow water in the North Atlantic and its multidecadal variability, Tellus A: Dyn. Meteorol. Oceanogr., 72(1), 1–10, https://doi.org/10.1080/16000870.2018.1565027, 2020.

Álvarez, M., Velo, A., Tanhua, T., Key, R., and van Heuven, S.: CARBON, TRACER AND ANCILLARY DATA IN THE MEDSEA, CARIMED: AN INTERNALLY CONSISTENT DATA PRODUCT FOR THE MEDITERRANEAN SEA., 2019.

Arístegui, J., & UTM-CSIC. HOTMIX Cruise, RV Sarmiento de Gamboa [Data set]. UTM-CSIC. https://doi.org/10.20351/29SG20140427, 2018.

Auger, P. A., Diaz, F., Ulses, C., Estournel, C., Neveux, J., Joux, F., Pujo-Pay, M., and Naudin, J. J.: Functioning of the planktonic ecosystem on the Gulf of Lions shelf (NW Mediterranean) during spring and its impact on the carbon deposition: a field data and 3-D modelling combined approach, Biogeosciences, 8, 3231–3261, https://doi.org/10.5194/bg-8-3231-2011, 2011.

Auger, P. A., Ulses, C., Estournel, C., Stemmann, L., Somot, S., and Diaz, F.: Interannual control of plankton communities by deep winter mixing and prey/predator interactions in the NW Mediterranean: Results from a 30-year 3D modeling study, Prog. Oceanogr., 124, 12–27, https://doi.org/10.1016/j.pocean.2014.04.004, 2014.

Batistić, M., Garić, R., & Molinero, J. C.: Interannual variations in Adriatic Sea zooplankton mirror shifts in circulation regimes in the Ionian Sea. Climate research, 61, 231-240, 2014.

Brasseur, P., Beckers, J. M., Brankart, J. M., and Schoenauer, R.: Seasonal temperature and salinity fields in the Mediterranean Sea: Climatological analyses of a historical data set, Deep Sea Res. Part Oceanogr. Res. Pap., 43, 159–192, https://doi.org/10.1016/0967-0637(96)00012-X, 1996.

Cardin, V., Civitarese, G., Hainbucher, D., Bensi, M., and Rubino, A.: Thermohaline properties in the Eastern Mediterranean in the last three decades: is the basin returning to the pre-EMT situation?, Ocean Sci., 11, 53–66, https://doi.org/10.5194/os-11-53-2015, 2015.

Christaki, U., Courties, C., Karayanni, H., Giannakourou, A., Maravelias, C., Kormas, K. Ar., and Lebaron, P.: Dynamic Characteristics of Prochlorococcus and Synechococcus Consumption by Bacterivorous Nanoflagellates, Microb. Ecol., 43, 341–352, https://doi.org/10.1007/s00248-002-2002-3, 2002.

Christaki, U., Van Wambeke, F., Lefevre, D., Lagaria, A., Prieur, L., Pujo-Pay, M., Grattepanche, J.-D., Colombet, J., Psarra, S., Dolan, J. R., Sime-Ngando, T., Conan, P., Weinbauer, M. G., and Moutin, T.: Microbial food webs and metabolic state across oligotrophic waters of the Mediterranean Sea during summer, Biogeosciences, 8, 1839–1852, https://doi.org/10.5194/bg-8-1839-2011, 2011.

Civitarese, G., Gačić, M., Batistić, M., Bensi, M., Cardin, V., Dulčić, J., and Menna, M.: The BiOS mechanism: history, theory, implications, *Prog. Oceanogr.*, 216, 103056, https://doi.org/10.1016/j.pocean.2023.103056, 2023.

Civitarese, G., Gačić, M., Lipizer, M., and Eusebi Borzelli, G. L.: On the impact of the Bimodal Oscillating System (BiOS) on the biogeochemistry and circulation of the Adriatic–Ionian system, *Prog. Oceanogr.*, 87, 1–10, https://doi.org/10.1016/j.pocean.2010.09.003, 2010.

Conan, P. and Durrieu De Madron, X.: PERLE2 cruise, Pourquoi pas ? R/V, https://doi.org/10.17600/18000865, 2019.

Copin-Montégut, C. and Bégovic, M.: Distributions of carbonate properties and oxygen along the water column (0–2000m) in the central part of the NW Mediterranean Sea (Dyfamed site): influence of winter vertical mixing on air–sea CO2 and O2 exchanges, Deep Sea Res. Part II Top. Stud. Oceanogr., 49, 2049–2066, https://doi.org/10.1016/S0967-0645(02)00027-9, 2002.

Coppola, L., Prieur, L., Taupier-Letage, I., Estournel, C., Testor, P., Lefevre, D., Belamari, S., LeReste, S., and Taillandier, V.: Observation of oxygen ventilation into deep waters through targeted deployment of multiple A rgo-

O_2 floats in the north-western Mediterranean Sea in 2013, J. Geophys. Res. Oceans, 122, 6325–6341, https://doi.org/10.1002/2016JC012594, 2017.

Coppola, L., Legendre, L., Lefevre, D., Prieur, L., Taillandier, V., and Diamond Riquier, E.: Seasonal and inter-annual variations of dissolved oxygen in the northwestern Mediterranean Sea (DYFAMED site), Prog. Oceanogr., 162, 187–201, https://doi.org/10.1016/j.pocean.2018.03.001, 2018.

Cossarini, G., Feudale, L., Teruzzi, A., Bolzon, G., Coidessa, G., Solidoro, C., Di Biagio, V., Amadio, C., Lazzari, P., Brosich, A., and Salon, S.: High-Resolution Reanalysis of the Mediterranean Sea Biogeochemistry (1999–2019), Front. Mar. Sci. 8, 741486, https://doi.org/10.3389/fmars.2021.741486, 2021.

Damien, P., Bosse, A., Testor, P., Marsaleix, P., and Estournel, C.: Modeling Postconvective Submesoscale Coherent Vortices in the Northwestern Mediterranean Sea, J. Geophys. Res. Oceans, 122, 9937–9961, https://doi.org/10.1002/2016JC012114, 2017.

Darmaraki, S., Denaxa, D., Theodorou, I., Livanou, E., Rigatou, D., Raitsos, E. D., Stavrakidis-Zachou, O., Dimarchopoulou, D., Bonino, G., McAdam, R., Organelli, E., Pitsouni, A., and Parasyris, A.: Marine heatwaves in the Mediterranean Sea: A literature review, Mediterr. Mar. Sci., 25(3), 586–620, https://doi.org/10.12681/mms.38392, 2024.

Di Biagio, V., Salon, S., Feudale, L., and Cossarini, G.: Subsurface oxygen maximum in oligotrophic marine ecosystems: mapping the interaction between physical and biogeochemical processes, https://doi.org/10.5194/bg-2022-70, ~~8 April~~ 2022.

Di Biagio, V., Martellucci, R., Menna, M., Teruzzi, A., Amadio, C., Mauri, E., and Cossarini, G.: Dissolved oxygen as an indicator of multiple drivers of the marine ecosystem: the southern Adriatic Sea case study, in: 7th edition of the Copernicus Ocean State Report (OSR7), edited by: von Schuckmann, K., Moreira, L., Le Traon, P.-Y., Grégoire, M., Marcos, M., Staneva, J., Brasseur, P., Garric, G., Lionello, P., Karstensen, J., and Neukermans, G., Copernicus Publications, State Planet, 1-osr7, 10, https://doi.org/10.5194/sp-1-osr7-10-2023, 2023.

D'Ortenzio, F. and Ribera d'Alcalà, M.: On the trophic regimes of the Mediterranean Sea: a satellite analysis, Biogeosciences, 6, 139–148, https://doi.org/10.5194/bg-6-139-2009, 2009.

D'Ortenzio, F., Antoine, D., and Marullo, S.: Satellite-driven modeling of the upper ocean mixed layer and air–sea CO2 flux in the Mediterranean Sea, Deep Sea Res. Part Oceanogr. Res. Pap., 55, 405–434, https://doi.org/10.1016/j.dsr.2007.12.008, 2008.

D'Ortenzio, F., Taillandier, V., Claustre, H., Coppola, L., Conan, P., Dumas, F., Durrieu Du Madron, X., Fourrier, M., Gogou, A., Karageorgis, A., Lefevre, D., Leymarie, E., Oviedo, A., Pavlidou, A., Poteau, A., Poulain, P. M., Prieur, L., Psarra, S., Puyo-Pay, M., Ribera d'Alcalà, M., Schmechtig, C., Terrats, L., Velaoras, D., Wagener, T., and Wimart-Rousseau, C.: BGC-Argo Floats Observe Nitrate Injection and Spring Phytoplankton Increase in the Surface Layer of Levantine Sea (Eastern Mediterranean), Geophys. Res. Lett., 48, e2020GL091649, https://doi.org/10.1029/2020GL091649, 2021.

Escudier, R., Clementi, E., Cipollone, A., Pistoia, J., Drudi, M., Grandi, A., Lyubartsev, V., Lecci, R., Aydogdu, A., Delrosso, D., Omar, M., Masina, S., Coppini, G., and Pinardi, N.: A High Resolution Reanalysis for the Mediterranean Sea, Front. Earth Sci., 9, 702285, https://doi.org/10.3389/feart.2021.702285, 2021.

Estournel, C., Kondrachoff, V., Marsaleix, P., and Vehil, R.: The plume of the Rhone: numerical simulation and remote sensing, Cont. Shelf Res., 17, 899–924, https://doi.org/10.1016/S0278-4343(96)00064-7, 1997.

Estournel, C., Broche, P., Marsaleix, P., Devenon, J.-L., Auclair, F., and Vehil, R.: The Rhone River Plume in Unsteady Conditions: Numerical and Experimental Results, Estuar. Coast. Shelf Sci., 53, 25–38, https://doi.org/10.1006/ecss.2000.0685, 2001.

Estournel, C., Zervakis, V., Marsaleix, P., Papadopoulos, A., Auclair, F., Perivoliotis, L., and Tragou, E.: Dense water formation and cascading in the Gulf of Thermaikos (North Aegean), from observations and modelling, Cont. Shelf Res., 25, 2366–2386, https://doi.org/10.1016/j.csr.2005.08.014, 2005.

Estournel, C., Testor, P., Damien, P., D'Ortenzio, F., Marsaleix, P., Conan, P., Kessouri, F., Durrieu De Madron, X., Coppola, L., Lellouche, J., Belamari, S., Mortier, L., Ulses, C., Bouin, M., and Prieur, L.: High resolution modeling of dense water formation in the north-western Mediterranean during winter 2012–2013: Processes and budget, J. Geophys. Res. Oceans, 121, 5367–5392, https://doi.org/10.1002/2016JC011935, 2016.

Estournel, C., Marsaleix, P., and Ulses, C.: A new assessment of the circulation of Atlantic and Intermediate Waters in the Eastern Mediterranean, Prog. Oceanogr., 198, 102673, https://doi.org/10.1016/j.pocean.2021.102673, 2021.

Fach, B. A., Örek, H., Salihoglu, I., Tezcan, D., Latif, M. A., and Salihoğlu, B.: Water mass variability and Levantine Intermediate Water formation in the eastern Mediterranean between 2015 and 2017, J. Geophys. Res. Oceans, 126, e2020JC016472, https://doi.org/10.1029/2020JC016472, 2021

Feucher, C., Portela, E., Kolodziejczyk, N., and Thierry, V.**:** Subpolar gyre decadal variability explains the recent oxygenation in the Irminger Sea, *Commun. Earth Environ.*, **3**, 279, https://doi.org/10.1038/s43247-022-00570-y, 2022

Fourrier, M.: Dataset used for CANYON-MED training and validation, https://doi.org/10.6084/M9.FIGSHARE.12452795.V2, 2020.

Fourrier, M., Coppola, L., D'Ortenzio, F., Migon, C., and Gattuso, J.: Impact of Intermittent Convection in the Northwestern Mediterranean Sea on Oxygen Content, Nutrients, and the Carbonate System, J. Geophys. Res. Oceans, 127, e2022JC018615, https://doi.org/10.1029/2022JC018615, 2022.

Gačić, M., Borzelli, G. L. E., Civitarese, G., Cardin, V., and Yari, S.: Can internal processes sustain reversals of the ocean upper circulation? The Ionian Sea example, Geophys. Res. Lett., 37, 2010GL043216, https://doi.org/10.1029/2010GL043216, 2010.

Garinet, A., Herrmann, M., Marsaleix, P., and Pénicaud, J.: Spurious numerical mixing under strong tidal forcing: a case study in the south-east Asian seas using the Symphonie model (v3.1.2), Geosci. Model Dev., 17, 6967–6986, https://doi.org/10.5194/gmd-17-6967-2024, 2024.

Grégoire, M., Raick, C., and Soetaert, K.: Numerical modeling of the central Black Sea ecosystem functioning during the eutrophication phase, Prog. Oceanogr., 76, 286–333, https://doi.org/10.1016/j.pocean.2008.01.002, 2008.

Grégoire, M., Garçon, V., Garcia, H., Breitburg, D., Isensee, K., Oschlies, A., Telszewski, M., Barth, A., Bittig, H. C., Carstensen, J., Carval, T., Chai, F., Chavez, F., Conley, D., Coppola, L., Crowe, S., Currie, K., Dai, M., Deflandre, B., Dewitte, B., Diaz, R., Garcia-Robledo, E., Gilbert, D., Giorgetti, A., Glud, R., Gutierrez, D., Hosoda, S., Ishii, M., Jacinto, G., Langdon, C., Lauvset, S. K., Levin, L. A., Limburg, K. E., Mehrtens, H., Montes, I., Naqvi, W., Paulmier, A., Pfeil, B., Pitcher, G., Pouliquen, S., Rabalais, N., Rabouille, C., Recape, V., Roman, M., Rose, K., Rudnick, D., Rummer, J., Schmechtig, C., Schmidtko, S., Seibel, B., Slomp, C., Sumalia, U. R., Tanhua, T., Thierry, V., Uchida, H., Wanninkhof, R., and Yasuhara, M.: A Global Ocean Oxygen Database and Atlas for Assessing and Predicting Deoxygenation and Ocean Health in the Open and Coastal Ocean, Front. Mar. Sci., 8, 724913, https://doi.org/10.3389/fmars.2021.724913, 2021.

Habib, J., Ulses, C., Estournel, C., Fakhri, M., Marsaleix, P., Pujo-Pay, M., Fourrier, M., Coppola, L., Mignot, A., Mortier, L., and Conan, P.: Seasonal and interannual variability of the pelagic ecosystem and of the organic carbon budget in the Rhodes Gyre (eastern Mediterranean): influence of winter mixing, Biogeosciences, 20, 3203–3228, https://doi.org/10.5194/bg-20-3203-2023, 2023.

Hainbucher, D., Álvarez, M., Astray Uceda, B., Bachi, G., Cardin, V., Celentano, P., Chaikakis, S., Chavez Montero, M. D. M., Civitarese, G., Fajar, N. M., Fripiat, F., Gerke, L., Gogou, A., Fernández Guallart, E., Gülk, B., Hassoun, A. E. R., Lange, N., Rochner, A., Santinelli, C., Steinhoff, T., Tanhua, T., Urbini, L., Velaoras, D., Wolf, F., and Welsch, A.: Variability and Trends in Physical and Biogeochemical Parameters of the Mediterranean Sea during a Cruise with RV MARIA S. MERIAN in March 2018, https://doi.org/10.5194/essd-2020-82, 7 July 2020.

Helm, K. P., Bindoff, N. L., and Church, J. A.: Observed decreases in oxygen content of the global ocean: ~~GLOBAL DECREASES IN OCEAN OXYGEN LEVELS~~Global decreases in ocean oxygen levels, Geophys. Res. Lett., 38, n/a-n/a, https://doi.org/10.1029/2011GL049513, 2011.

Herrmann, M., Somot, S., Sevault, F., Estournel, C., and Déqué, M.: Modeling the deep convection in the northwestern Mediterranean Sea using an eddy-permitting and an eddy-resolving model: Case study of winter 1986–1987, J. Geophys. Res. Oceans, 113, 2006JC003991, https://doi.org/10.1029/2006JC003991, 2008.

Herrmann, M., Diaz, F., Estournel, C., Marsaleix, P., and Ulses, C.: Impact of atmospheric and oceanic interannual variability on the Northwestern Mediterranean Sea pelagic planktonic ecosystem and associated carbon cycle: Interannual Variability Impact on Nwms, J. Geophys. Res. Oceans, 118, 5792–5813, https://doi.org/10.1002/jgrc.20405, 2013.

Houpert, L., Testor, P., Durrieu De Madron, X., Somot, S., D'Ortenzio, F., Estournel, C., and Lavigne, H.: Seasonal cycle of the mixed layer, the seasonal thermocline and the upper-ocean heat storage rate in the Mediterranean Sea derived from observations, Prog. Oceanogr., 132, 333–352, https://doi.org/10.1016/j.pocean.2014.11.004, 2015.

Jangir, B., Mishra, A. K., and Strobach, E.: The interplay between medicanes and the Mediterranean Sea in the presence of sea surface temperature anomalies, Atmos. Res., 310, 107625, https://doi.org/10.1016/j.atmosres.2024.107625, 2024.

Jangir, B., Reale, M., Menna, M., Mishra, A. K., Marellucci, R., Cossarini, G., et al.: The response of the physical and biogeochemical marine environment to the passage of Mediterranean cyclones in the presence of eddies, gyres, and marine heat waves, J. Geophys. Res. Oceans, 131, e2025JC023151, doi:10.1029/2025JC023151, 2026.

Josey, S. A., Gulev, S., and Yu, L.: Exchanges through the ocean surface, in: *Ocean Circulation and Climate*, 2nd edn., edited by: Siedler, G., Griffies, S. M., Gould, J., and Church, J. A., Academic Press, 115–140, https://doi.org/10.1016/B978-0-12-391851-2.00005-2, 2013.

Keeling, R. F., Körtzinger, A., and Gruber, N.: Ocean deoxygenation in a warming world, Annu. Rev. Mar. Sci., 2, 199–229, https://doi.org/10.1146/annurev.marine.010908.163855, 2010.

Kessouri, F., Ulses, C., Estournel, C., Marsaleix, P., Severin, T., Pujo-Pay, M., Caparros, J., Raimbault, P., Pasqueron De Fommervault, O., D'Ortenzio, F., Taillandier, V., Testor, P., and Conan, P.: Nitrogen and Phosphorus Budgets in the Northwestern Mediterranean Deep Convection Region, J. Geophys. Res. Oceans, 122, 9429–9454, https://doi.org/10.1002/2016JC012665, 2017.

Kessouri, F., Ulses, C., Estournel, C., Marsaleix, P., D'Ortenzio, F., Severin, T., Taillandier, V., and Conan, P.: Vertical Mixing Effects on Phytoplankton Dynamics and Organic Carbon Export in the Western Mediterranean Sea, J. Geophys. Res. Oceans, 123, 1647–1669, https://doi.org/10.1002/2016JC012669, 2018.

Klein, B., Roether, W., Kress, N., Manca, B. B., Ribera d'Alcala, M., Souvermezoglou, E., Theocharis, A., Civitarese, G., and Luchetta, A.: Accelerated oxygen consumption in eastern Mediterranean deep waters following the recent changes in thermohaline circulation, J. Geophys. Res. Oceans, 108, 2002JC001454, https://doi.org/10.1029/2002JC001454, 2003.

Kolodziejczyk, N., Portela, E., Thierry, V., and Prigent, A.: ISASO2: recent trends and regional patterns of ocean dissolved oxygen change, Earth Syst. Sci. Data, 16, 5191–5206, https://doi.org/10.5194/essd-16-5191-2024, 2024.

Körtzinger, A., Schimanski, J., Send, U., and Wallace, D.: The Ocean Takes a Deep Breath, Science, 306, 1337–1337, https://doi.org/10.1126/science.1102557, 2004.

Körtzinger, A., Send, U., Lampitt, R. S., Hartman, S., Wallace, D. W. R., Karstensen, J., Villagarcia, M. G., Llinás, O., and DeGrandpre, M. D.: The seasonal p CO_2 cycle at 49°N/16.5°W in the northeastern Atlantic Ocean and what it tells us about biological productivity, J. Geophys. Res. Oceans, 113, 2007JC004347, https://doi.org/10.1029/2007JC004347, 2008.

Kress, N. and Herut, B.: Spatial and seasonal evolution of dissolved oxygen and nutrients in the Southern Levantine Basin (Eastern Mediterranean Sea): chemical characterization of the water masses and inferences on the N:P ratios, Deep Sea Res. Part Oceanogr. Res. Pap., 48, 2347–2372, https://doi.org/10.1016/S0967-0637(01)00022-X, 2001.

Kress, N., Manca, B. B., Klein, B., and Deponte, D.: Continuing influence of the changed thermohaline circulation in the eastern Mediterranean on the distribution of dissolved oxygen and nutrients: Physical and chemical characterization of the water masses, J. Geophys. Res. Oceans, 108, 2002JC001397, https://doi.org/10.1029/2002JC001397, 2003.

Kress, N., Gertman, I., and Herut, B.: Temporal evolution of physical and chemical characteristics of the water column in the Easternmost Levantine basin (Eastern Mediterranean Sea) from 2002 to 2010, J. Mar. Syst., 135, 6–13, https://doi.org/10.1016/j.jmarsys.2013.11.016, 2014.

Lagaria, A., Psarra, S., Lefèvre, D., Van Wambeke, F., Courties, C., Pujo-Pay, M., Oriol, L., Tanaka, T., and Christaki, U.: The effects of nutrient additions on particulate and dissolved primary production and metabolic state in surface waters of three Mediterranean eddies, Biogeosciences, 8, 2595–2607, https://doi.org/10.5194/bg-8-2595-2011, 2011.

Large, W. G., McWilliams, J. C., and Doney, S. C.: Oceanic vertical mixing: A review and a model with a nonlocal boundary layer parameterization, *Rev. Geophys.*, 32, 363–403, https://doi.org/10.1029/94RG01872, 1994.

Lascaratos, A. and Nittis, K.: A high-resolution three-dimensional numerical study of intermediate water formation in the Levantine Sea, J. Geophys. Res. Oceans, 103, 18497–18511, https://doi.org/10.1029/98JC01196, 1998.

Lascaratos, A., Roether, W., Nittis, K., and Klein, B.: Recent changes in deep water formation and spreading in the eastern Mediterranean Sea: a review, Prog. Oceanogr., 44, 5–36, https://doi.org/10.1016/S0079-6611(99)00019-1, 1999.

Lavigne, H., D'Ortenzio, F., Migon, C., Claustre, H., Testor, P., d'Alcalà, M. R., Lavezza, R., Houpert, L., and Prieur, L.: Enhancing the comprehension of mixed layer depth control on the Mediterranean phytoplankton phenology: Mediterranean Phytoplankton Phenology, J. Geophys. Res. Oceans, 118, 3416–3430, https://doi.org/10.1002/jgrc.20251, 2013.

Lavigne, H., D'Ortenzio, F., Ribera D'Alcalà, M., Claustre, H., Sauzède, R., and Gacic, M.: On the vertical distribution of the chlorophyll a concentration in the Mediterranean Sea: a basin-scale and seasonal approach, Biogeosciences, 12, 5021–5039, https://doi.org/10.5194/bg-12-5021-2015, 2015.

Legendre, L. and Rassoulzadegan, F.: Plankton and nutrient dynamics in marine waters, Ophelia, 41, 153–172, https://doi.org/10.1080/00785236.1995.10422042, 1995.

Malanotte-Rizzoli, P., Manca, B. B., Marullo, S., Ribera D' Alcala', M., Roether, W., Theocharis, A., Bergamasco, A., Budillon, G., Sansone, E., Civitarese, G., Conversano, F., Gertman, I., Hernt, B., Kress, N., Kioroglou, S., Kontoyannis, H., Nittis, K., Klein, B., Lascaratos, A., Latif, M. A., Ozsoy, E., Robinson, A. R., Santoleri, R., Viezzoli, D., and Kovacevic, V.: The Levantine Intermediate Water Experiment (LIWEX) Group: Levantine basin—A laboratory for multiple water mass formation processes, J. Geophys. Res. Oceans, 108, 2002JC001643, https://doi.org/10.1029/2002JC001643, 2003.

Malanotte-Rizzoli, P., Artale, V., Borzelli-Eusebi, G. L., Brenner, S., Crise, A., Gacic, M., Kress, N., Marullo, S., Ribera d'Alcalà, M., Sofianos, S., Tanhua, T., Theocharis, A., Alvarez, M., Ashkenazy, Y., Bergamasco, A., Cardin, V., Carniel, S., Civitarese, G., D'Ortenzio, F., Font, J., Garcia-Ladona, E., Garcia-Lafuente, J. M., Gogou, A., Gregoire, M., Hainbucher, D., Kontoyannis, H., Kovacevic, V., Kraskapoulou, E., Kroskos, G., Incarbona, A., Mazzocchi, M. G., Orlic, M., Ozsoy, E., Pascual, A., Poulain, P.-M., Roether, W., Rubino, A., Schroeder, K., Siokou-Frangou, J., Souvermezoglou, E., Sprovieri, M., Tintoré, J., and Triantafyllou, G.: Physical forcing and physical/biochemical variability of the Mediterranean Sea: a review of unresolved issues and directions for future research, Ocean Sci., 10, 281–322, https://doi.org/10.5194/os-10-281-2014, 2014.

Manca, B., Burca, M., Giorgetti, A., Coatanoan, C., Garcia, M.-J., and Iona, A.: Physical and biochemical averaged vertical profiles in the Mediterranean regions: an important tool to trace the climatology of water masses and to validate incoming data from operational oceanography, J. Mar. Syst., 48, 83–116, https://doi.org/10.1016/j.jmarsys.2003.11.025, 2004.

Manca, B. B., Ibello, V., Pacciaroni, M., Scarazzato, P., & Giorgetti, A.: Ventilation of deep waters in the Adriatic and Ionian Seas following changes in thermohaline circulation of the Eastern Mediterranean. Climate Research, 31, 239-256, 2006.

Many, G., Ulses, C., Estournel, C., and Marsaleix, P.: Particulate organic carbon dynamics in the Gulf of Lion shelf (NW Mediterranean) using a coupled hydrodynamic–biogeochemical model, Biogeosciences, 18, 5513–5538, https://doi.org/10.5194/bg-18-5513-2021, 2021.

Marsaleix, P., Estournel, C., Kondrachoff, V., and Vehil, R.: A numerical study of the formation of the Rhône River plume, J. Mar. Syst., 14, 99–115, https://doi.org/10.1016/S0924-7963(97)00011-0, 1998.

Marsaleix, P., Auclair, F., and Estournel, C.: Considerations on Open Boundary Conditions for Regional and Coastal Ocean Models, J. Atmospheric Ocean. Technol., 23, 1604–1613, https://doi.org/10.1175/JTECH1930.1, 2006.

Marsaleix, P., Auclair, F., Floor, J. W., Herrmann, M. J., Estournel, C., Pairaud, I., and Ulses, C.: Energy conservation issues in sigma-coordinate free-surface ocean models, Ocean Model., 20, 61–89, https://doi.org/10.1016/j.ocemod.2007.07.005, 2008.

Martínez-Pérez, A. M., Osterholz, H., Nieto-Cid, M., Álvarez, M., Dittmar, T., and Álvarez-Salgado, X. A.: Molecular composition of dissolved organic matter in the Mediterranean Sea, Limnol. Oceanogr., 62, 2699–2712, https://doi.org/10.1002/lno.10600, 2017.

Mavropoulou, A.-M., Vervatis, V., and Sofianos, S.: Dissolved oxygen variability in the Mediterranean Sea, J. Mar. Syst., 208, 103348, https://doi.org/10.1016/j.jmarsys.2020.103348, 2020.

Mayot, N., D'Ortenzio, F., Ribera d'Alcalà, M., Lavigne, H., and Claustre, H.: Interannual variability of the Mediterranean trophic regimes from ocean color satellites, Biogeosciences, 13, 1901–1917, https://doi.org/10.5194/bg-13-1901-2016, 2016.

Menna, M., Martellucci, R., Reale, M., Cossarini, G., Salon, S., Notarstefano, G., et al. (2023). A case study of impacts of an extreme weather system on the Mediterranean Sea circulation features: Medicane Apollo (2021). Scientific Reports, 13(1), 3870. https://doi.org/10.1038/s41598-023-29942-w

Menna, M., Poulain, P.-M., Zodiatis, G., and Gertman, I.: On the decadal variability of the North Ionian Gyre and its impact on the thermohaline properties of the Levantine Intermediate Water, Prog. Oceanogr., 200, 102709, https://doi.org/10.1016/j.pocean.2021.102709, 2022.

Mikolajczak, G., Estournel, C., Ulses, C., Marsaleix, P., Bourrin, F., Martín, J., Pairaud, I., Puig, P., Leredde, Y., Many, G., Seyfried, L., and Durrieu De Madron, X.: Impact of storms on residence times and export of coastal waters during a mild autumn/winter period in the Gulf of Lion, Cont. Shelf Res., 207, 104192, https://doi.org/10.1016/j.csr.2020.104192, 2020.

Millot, C. and Taupier-Letage, I.: Circulation in the Mediterranean Sea, in: The Mediterranean Sea, vol. 5K, edited by: Saliot, A., Springer Berlin Heidelberg, Berlin, Heidelberg, 29–66, https://doi.org/10.1007/b107143, 2005.

Moutin, T. and Raimbault, P.: Primary production, carbon export and nutrients availability in western and eastern Mediterranean Sea in early summer 1996 (MINOS cruise), J. Marine Syst., 33–34, 273–288, https://doi.org/10.1016/S0924-7963(02)00062- 3, 2002

Ozer, T., Gertman, I., Kress, N., Silverman, J., and Herut, B.: Interannual thermohaline (1979–2014) and nutrient (2002–2014) dynamics in the Levantine surface and intermediate water masses, SE Mediterranean Sea, Glob. Planet. Change, 151, 60–67, https://doi.org/10.1016/j.gloplacha.2016.04.001, 2016.

Ozer, T., Gertman, I., Gildor, H., Goldman, R., and Herut, B.: Evidence for recent thermohaline variability and processes in the deep water of the Southeastern Levantine Basin, Mediterranean Sea, Deep Sea Res. Part II Top. Stud. Oceanogr., 171, 104651, https://doi.org/10.1016/j.dsr2.2019.104651, 2020.

Ozer, T., Rahav, E., Gertman, I., Sisma-Ventura, G., Silverman, J., and Herut, B.: Relationship between thermohaline and biochemical patterns in the levantine upper and intermediate water masses, Southeastern Mediterranean Sea (2013–2021), Front. Mar. Sci., 9, 958924, https://doi.org/10.3389/fmars.2022.958924, 2022.

Pirro, A., Menna, M., Mauri, E., Laxenaire, R., Salon, S., Bosse, A., Martellucci, R., Viboud, S., Valran, T., Hayes, D., Speich, S., Poulain, P.-M., and Negretti, M. E.: Rossby waves driven by the Mid Mediterranean Jet impact the Eastern Mediterranean mesoscale dynamics, *Sci. Rep.*, **14**, 29598, https://doi.org/10.1038/s41598-024-80293-6, 2024.

Powley, H. R., Krom, M. D., and Van Cappellen, P.: Circulation and oxygen cycling in the Mediterranean Sea: Sensitivity to future climate change: OXYGEN CYCLING IN THE MEDITERRANEAN SEA, J. Geophys. Res. Oceans, 121, 8230–8247, https://doi.org/10.1002/2016JC012224, 2016.

Reale, M., Giordano, F., Biagio, V. D., Cossarini, G., & Salon, S. (2026). Synoptic features driving the CO_2 sink in the Mediterranean Sea in winter. Journal of Geophysical Research: Atmospheres, 131(2), e2025JD044310. https://doi.org/10.1029/2025JD044310

Regaudie-de-Gioux, A., Vaquer-Sunyer, R., and Duarte, C. M.: Patterns in planktonic metabolism in the Mediterranean Sea, 2009.

Robinson, A. R. and Golnaraghi, M.: Circulation and dynamics of the Eastern Mediterranean Sea; quasi-synoptic data-driven simulations, Deep Sea Res. Part II Top. Stud. Oceanogr., 40, 1207–1246, https://doi.org/10.1016/0967-0645(93)90068-X, 1993.

Roether, W. and Schlitzer, R.: Eastern Mediterranean deep water renewal on the basis of chlorofluoromethane and tritium data, Dyn. Atmospheres Oceans, 15, 333–354, https://doi.org/10.1016/0377-0265(91)90025-B, 1991.

Roether, W. and Well, R.: Oxygen consumption in the Eastern Mediterranean, Deep Sea Res. Part Oceanogr. Res. Pap., 48, 1535–1551, https://doi.org/10.1016/S0967-0637(00)00102-3, 2001.

Salihoğlu, İ., Saydam, C., Baştürk, Ö., Yilmaz, K., Göçmen, D., Hatipoğlu, E., and Yilmaz, A.: Transport and distribution of nutrients and chlorophyll-a by mesoscale eddies in the northeastern Mediterranean, Mar. Chem., 29, 375–390, https://doi.org/10.1016/0304-4203(90)90024-7, 1990.

Schlitzer, R., Roether, W., Oster, H., Junghans, H.-G., Hausmann, M., Johannsen, H., and Michelato, A.: Chlorofluoromethane and oxygen in the Eastern Mediterranean, Deep Sea Res. Part Oceanogr. Res. Pap., 38, 1531–1551, https://doi.org/10.1016/0198-0149(91)90088-W, 1991.

Schmidtko, S., Stramma, L., and Visbeck, M.: Decline in global oceanic oxygen content during the past five decades, Nature, 542, 335–339, https://doi.org/10.1038/nature21399, 2017.

Schneider, A., Tanhua, T., Roether, W., and Steinfeldt, R.: Changes in ventilation of the Mediterranean Sea during the past 25 year, Ocean Sci., 10, 1–16, https://doi.org/10.5194/os-10-1-2014, 2014.

Siokou-Frangou, I., Bianchi, M., Christaki, U., Christou, E. D., Giannakourou, A., Gotsis, O., Ignatiades, L., Pagou, K., Pitta, P., Psarra, S., Souvermezoglou, E., Van Wambeke, F., and Zervakis, V.: Carbon flow in the planktonic food web along a gradient of oligotrophy in the Aegean Sea (Mediterranean Sea), J. Mar. Syst., 33–34, 335–353, https://doi.org/10.1016/S0924-7963(02)00065-9, 2002.

Siokou-Frangou, I., Christaki, U., Mazzocchi, M. G., Montresor, M., Ribera d'Alcalá, M., Vaqué, D., and Zingone, A.: Plankton in the open Mediterranean Sea: a review, Biogeosciences, 7, 1543–1586, https://doi.org/10.5194/bg-7-1543-2010, 2010.

Sisma-Ventura, G., Yam, R., Kress, N., and Shemesh, A.: Water column distribution of stable isotopes and carbonate properties in the South-eastern Levantine basin (Eastern Mediterranean): Vertical and temporal change, J. Mar. Syst., 158, 13–25, https://doi.org/10.1016/j.jmarsys.2016.01.012, 2016.

Sisma-Ventura, G., Kress, N., Silverman, J., Gertner, Y., Ozer, T., Biton, E., Lazar, A., Gertman, I., Rahav, E., and Herut, B.: Post-eastern Mediterranean Transient Oxygen Decline in the Deep Waters of the Southeast Mediterranean Sea Supports Weakening of Ventilation Rates, Front. Mar. Sci. 7, 598686, https://doi.org/10.3389/fmars.2020.598686, 2021.

Stendardo, I., and Gruber, N.: Oxygen trends over five decades in the North Atlantic, J. Geophys. Res. Oceans, 117, C11004, https://doi.org/10.1029/2012JC007909, 2012.

Stramma, L. and Schmidtko, S.: Spatial and Temporal Variability of Oceanic Oxygen Changes and Underlying Trends, Atmosphere-Ocean, 59, 122–132, https://doi.org/10.1080/07055900.2021.1905601, 2021.

Sur, H., Ozsoy, E., and Unluata, U.: Simultaneous deep and intermediate depth convection in the northern levantine sea, winter 1992, Oceanol. Acta, 16, 1993.

Tanhua, T.: Hydrochemistry of water samples during METEOR cruise M83/1, https://doi.org/10.1594/PANGAEA.821729, 2013.

Tanhua, T., Hainbucher, D., Schroeder, K., Cardin, V., Álvarez, M., and Civitarese, G.: The Mediterranean Sea system: a review and an introduction to the special issue, Ocean Sci., 9, 789–803, https://doi.org/10.5194/os-9-789-2013, 2013.

~~Theocharis, A., Georgopoulos, D., Lascaratos, A., and Nittis, K.: Water masses and circulation in the central region of the Eastern Mediterranean: Eastern Ionian, South Aegean and Northwest Levantine, 1986–1987, Deep Sea Res. Part II Top. Stud. Oceanogr., 40, 1121–1142, https://doi.org/10.1016/0967-0645(93)90064-T, 1993.~~

Thierry, V., Bittig, H., and The Argo-Bgc Team: Argo quality control manual for dissolved oxygen concentration, Argo-BGC group, https://doi.org/10.13155/46542, 2021.

Trinh, N. B., Herrmann, M., Ulses, C., Marsaleix, P., Duhaut, T., To Duy, T., Estournel, C., and Shearman, R. K.: New insights into the South China Sea throughflow and water budget seasonal cycle: evaluation and analysis of a high-resolution configuration of the ocean model SYMPHONIE version 2.4, Geosci. Model Dev., 17, 1831–1867, https://doi.org/10.5194/gmd-17-1831-2024, 2024.

Tugrul, S., Besiktepe, T., and Salihoglu, I.: Nutrient exchange fluxes between the Aegean and Black Seas through the Marmara Sea, Mediterr. Mar. Sci., 3, 33, https://doi.org/10.12681/mms.256, 2002.

Ulses, C., Estournel, C., Puig, P., Durrieu De Madron, X., and Marsaleix, P.: Dense shelf water cascading in the northwestern Mediterranean during the cold winter 2005: Quantification of the export through the Gulf of Lion and the Catalan margin, Geophys. Res. Lett., 35, 2008GL033257, https://doi.org/10.1029/2008GL033257, 2008.

Ulses, C., Auger, P. -A., Soetaert, K., Marsaleix, P., Diaz, F., Coppola, L., Herrmann, M. J., Kessouri, F., and Estournel, C.: Budget of organic carbon in the North- Western Mediterranean open sea over the period 2004–2008 using 3-D coupled physical-biogeochemical modeling, J. Geophys. Res. Oceans, 121, 7026–7055, https://doi.org/10.1002/2016JC011818, 2016.

Ulses, C., Estournel, C., Fourrier, M., Coppola, L., Kessouri, F., Lefèvre, D., and Marsaleix, P.: Oxygen budget of the north-western Mediterranean deep- convection region, Biogeosciences, 18, 937–960, https://doi.org/10.5194/bg-18-937-2021, 2021.

Ulses, C., Estournel, C., Marsaleix, P., Soetaert, K., Fourrier, M., Coppola, L., Lefèvre, D., Touratier, F., Goyet, C., Guglielmi, V., Kessouri, F., Testor, P., and Durrieu De Madron, X.: Seasonal dynamics and annual budget of dissolved inorganic carbon in the northwestern Mediterranean deep-convection region, Biogeosciences, 20, 4683–4710, https://doi.org/10.5194/bg-20-4683-2023, 2023.

Velaoras, D., Krokos, G., Nittis, K., and Theocharis, A.: Dense intermediate water outflow from the ~~C retan S ea~~Cretan Sea: A salinity driven, recurrent phenomenon, connected to thermohaline circulation changes, J. Geophys. Res. Oceans, 119, 4797–4820, https://doi.org/10.1002/2014JC009937, 2014.

Wanninkhof, R. and McGillis, W. R.: A cubic relationship between air-sea CO_2 exchange and wind speed, Geophys. Res. Lett., 26, 1889–1892, https://doi.org/10.1029/1999GL900363, 1999.

Wolf, M. K., Hamme, R. C., Gilbert, D., Yashayaev, I., and Thierry, V.: Oxygen Saturation Surrounding Deep Water Formation Events in the Labrador Sea From Argo-O_2 Data, Glob. Biogeochem. Cycles, 32, 635–653, ~~://~~:https//doi.org/10.1002/2017GB005829, 2018.

Wu, Y., Zheng, Z., Chen, X., Huang, F., Liu, C., and Tang, D.: Amplified warming accelerates deoxygenation in the Arctic Ocean, Nat. Clim. Chang., 15, 859–865, https://doi.org/10.1038/s41558-025-02376-0, 2025.

Ziveri, P. and Grelaud, M.: Physical oceanography during Ángeles Alvariño cruise MedSeA2013, https://doi.org/10.1594/PANGAEA.846067, 2015.

~~Zodiatis, G.: Circulation of the Cretan sea-water masses (Eastern Mediterranean Sea), Oceanol. Acta, 16, 107–114, 1993.~~